Crystallography Reports, Vol. 44, No. 4, 1999, pp. 686–709. Translated from Kristallografiya, Vol. 44, No. 4, 1999, pp. 736–760.

HISTORY OF SCIENCE
REVIEWS

State-of-Art and Perspectives of the Bond-Valence Model in Inorganic Crystal Chemistry

V. S. Urusov and I. P. Orlov

Moscow State University, Vorob'evy gory, Moscow, 119489 Russia

Received December 10, 1997

Abstract—The bond valence method (BVM) is one of modern methods for predicting bond lengths in crystal structures based on the modified second Pauling rule, which requires the exact fulfillment of the valence balance with due regard for the empirical bond valence–bond length relations. The review includes the detailed analysis of the mathematical apparatus of the method, its limitations, and also its program implementation. Various modifications of the BVM procedure suggested by the authors are analyzed. A number of examples of modeling are given. In most of the cases, the error in prediction of interatomic distances does not exceed 5–8%. Much attention is also given to other possible applications of the method in crystal chemistry. Among them, of great importance is the prediction of coordination-polyhedron distortion based on the use of the distortion theorem, the determination of the valence of atoms from the corresponding structural data, the refinement of the bond network, and also the analysis of geometrical strains in structures.

LIST OF CONTENTS

INTRODUCTION

It is well known that all the main notions used for the description of chemical bonding between atoms used in modern theoretical crystal chemistry, such as those of atomic and ionic radii, polarizabilities, electronegativities, etc. [1], are not rigorously determined constants but rather some effective quantities determined and evaluated by various methods and estimates. However, this does not hinder numerous successful applications of these notions under the condition of their consistency and the fulfillment of some important requirements (e.g., the sums of atomic radii should be as close as possible to the values of the measured interatomic distances).

Among most popular crystallochemical techniques, the special attention is recently given to the bond-valence model, which allows the interpretation and prediction of bond lengths for most inorganic crystals and minerals. The present review is aimed at closing the gap in Russian publications on inorganic chemistry, which, until today, have not given sufficient attention to this important concept.

1063-7745/99/4404-0686$15.00 © 1999 МАИК "Наука/Interperiodica"

I. INTERATOMIC DISTANCES AND BOND VALENCE

1.1 Modification of the Second Pauling Rule

The most well-known rule of the five Pauling rules describing the structure of ionic crystals is the second one,

$$V_j \cong \sum_i^{\nu} V_i/\nu_i = \sum s_i, \qquad (1)$$

which postulates that in a stable structure, the charge (valence) V_j of each anion has a tendency to be compensated with the valence strengths $s_i = V_i/\nu$ (where ν is the coordination number) of all the cations forming a coordination polyhedron around the given anion. The second Pauling rule is rigorously fulfilled only for simple highly symmetric structures with undistorted chemically-homogeneous coordination polyhedra. In most instances, this rule is only an approximate condition deviating from the rigorous equality within ±10%. Indeed, for oxygen atoms in silicate structures, the deviations from (1) are usually within 1/6 of the valence unit, in other words, the total sum of the valence strengths of cations does not exceed 1.8–2.2.

However, even for stable synthetic compounds, the deviations from postulate (1) can attain 40% and, for less stable compounds, even 50%. Thus, the bridge oxygen atom in a disulfite S_2O_7 group is "oversaturated" (by one valence unit). In this situation, the second Pauling rule becomes somewhat indeterminate. To confirm its validity one should invoke the notion of the valence strength described by (1). The dependence between the value of the valence strength s and the bond length R was first indicated in the early fifties [2, 3]. In 1970, G. Donnay and R. Allmann [4] suggested to use the notion "bond valence" instead of the "valence strength" suggested by Pauling. Bond valence and bond length are related by the inverse power relationship

$$s_{ij} = (R_{ij}/R_1)^{-N}, \qquad (2)$$

where N and R_1 are the empirical constants, with R_1 being correspondent to the bond length having a unit valence ($s_{ij} = 1$). This relationship proved to be more appropriate than the linear [5] and the parabolic [6] correlations between the bond length and the deviation Δs from the Pauling valence strength. The values of R_1 and N were empirically determined elsewhere [7–10].

Another expression for the dependence $s(R)$ suggested in [11, 12] has the exponential form:

$$s_{ij} = \exp[(R_{1j} - R_{ij})/b], \qquad (3)$$

where, similar to (2), the quantity R_1 has the sense of a unit valence ($s_{ij} = 1$), whereas the parameter b varies within a narrow range from 0.32 to 0.48 Å. We should like to remind here that a similar logarithmic expression for the dependence between the length R and the order n of the C–C bonds was suggested by Pauling as far back as 1947 [13]. Pauling determined the empirical value of b as $b = 0.31$ Å and assumed that the logarithmic expression should also be valid for various covalent and metal crystals. Such a close correspondence between the dependences $s(R)$ and $n(R)$ suggested by Pauling is explained by the fact that, similar to the bond order, the bond valence can be interpreted as numbers of electron pairs per bond [14].

Later, it was also assumed that b can be equated to the average (universal) value 0.37 Å [15]. Then, equation (3) has only one empirical parameter—the length of the unit-valence bond, R_1. The values of this parameter for various bonds were determined by processing numerous empirical data from the Inorganic Crystals Structure Database [16] tabulated in [15, 17]. It is believed that the accuracy of the R_1 evaluation is about 0.02 Å, although for many oxides and fluorides this accuracy should be somewhat higher [17]. Thus, the model under question can be used for predicting bond lengths with an error not exceeding several hundredths of angstrom. It is important that the values of the parameter R_1 calculated by (2) and (3) are very close. These values for various atomic pairs are indicated in Appendix 1.

One can see that with an increase of the ordinal number of an element within a group of the Periodic System, the value of R_1 noticeably increases. As was shown in [13, 18], the values of R_1 can be represented as sums of covalent radii with due regard for the correction for different electronegativities of the bonded atoms.

As a result, modifying the second Pauling rule, I.D. Brown [10] obtained the bond-valence sum rule (BVS). Thus, equation (1) takes the form

$$V_j = \sum_i^{\nu} s_{ij}(R_{ij}), \qquad (4)$$

in which the approximate equality is changed for the exact one, and the Pauling valence strength s_i is changed for the bond valence (BV) s_{ij}. Moreover, it should be emphasized that, unlike (1), equation (4) should be rigorously fulfilled for both cations and anions.

Another important remark reduces to that, within the framework of the bond-valence model, the terms "cation" and "anion" differ in that the former are more electropositive and the latter are more electronegative atoms forming chemical bonds. These bonds are not necessarily ionic. The model is equally applicable to all inorganic compounds including those characterized by metallic bonding [18]. The "experimental" s_{ij} values

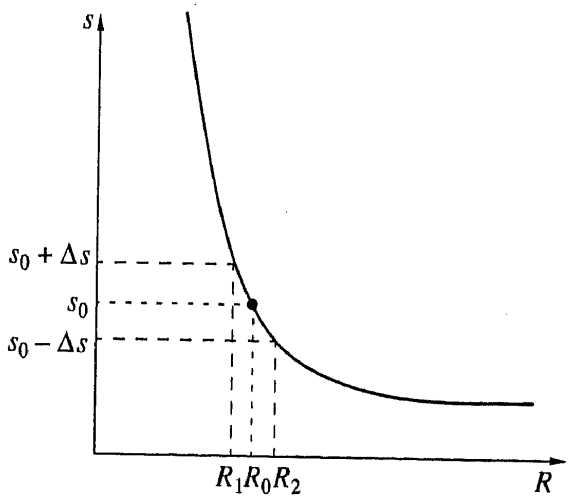

Fig. 1. Correlation between the bond length R and the bond valence s illustrating the geometric proof of the distortion theorem.

can be calculated from the experimental bond lengths. The measure of the difference between the "experimental" valence $\sum s_{ij}$ and the expected value V_j,

$$\Delta V_j = V_j - \sum_i s_{ij} \quad (5)$$

can be used for calculating the reliability factor of the structure (the value ΔV_j for all j atoms in the formula unit):

$$D(\Delta V) = \langle \Delta V \rangle^{1/2}. \quad (6)$$

The experimental errors in the determination of the atomic coordinates and bond lengths can result in the factor D equal to about one valence unit. Higher values of this factor indicate that either the structure determination is unreliable or the crystal under question is unstable.

1.2 Distortion Theorem

If the arrangement of the atoms in the crystal structure obeys condition (4), then an important distortion theorem [19, 20] is valid. The theorem states that any deviation of bond lengths from their average value results in an increase of the average bond length under the condition that the average bond valence (or the sum of bond valences) remains constant. This theorem was proved by Brown who proceeded from the geometrical form of the bond length–bond valence dependence [19, 20] (Fig. 1).

It is seen from Fig. 1 that an increase of the valence s_0 of one of two initially equivalent bonds by Δs and a decrease of the second bond by $-\Delta s$ elongates the second bond length to a larger extent than it reduces the first one, i.e., $R_2 - R_0 > R_0 - R_1$. Thus, the average bond length $(R_2 + R_1)/2$ increases.

The distortion theorem can readily be proven in the analytical form. With this aim, determine the slope of the curve $s(R)$ by differentiating equation (3):

$$ds_{ij}/dR_{ij} = -(1/b)\exp\left(\frac{R_1 - R_{ij}}{b}\right) = -(1/b)s_{ij}. \quad (7)$$

First, consider the chain B–A–B consisting of two equivalent A–B bonds which are characterized by the bond valence s and the bond length R. Then, we assume that both bonds change their lengths and valences, but in such a way that the total sum of the bond valences remains constant

$$2s + \Delta s + \Delta s' = 2s,$$

so that

$$\Delta s = -\Delta s'.$$

Thus, one can write for a distorted chain of the B–A–B' bonds

$$s(A-B) = s + \Delta s \text{ and } R(A-B) = R + \Delta R,$$

$$s(A-B') = s + \Delta s' \text{ and } R(A-B') = R + \Delta R'.$$

Now, assume that $\Delta s > 0$. Then, obviously, $\Delta R < 0$ and $\Delta R' > 0$. Proceeding to the finite differences, we obtain from (7):

$$\Delta s = -(1/b)(s + \Delta s)\Delta R,$$

$$-\Delta s = -(1/b)(s - \Delta s)\Delta R'.$$

Summing the two above equations, we have

$$\Delta R + \Delta R' = (\Delta s/s)(\Delta R'/\Delta R). \quad (8)$$

Taking into account that $\Delta s/s > 0$ and $(\Delta R' - \Delta R) > 0$, we can conclude that

$$\Delta R + \Delta R' > 0.$$

In other words, as a result of distortion, the average bond length, $R_{av} = (R + R')/2$, increases.

Now consider the structural unit or a polyhedron AB_ν. Let this polyhedron be distorted in such a way that it becomes possible to divide n bonds into two groups, $\nu = \nu_1 + \nu_2$, containing the bonds of lengths R_1 and R_2, respectively. The corresponding differences between the bond valences and the bond lengths between these two groups of bond valences and lengths and those for a regular polyhedron are Δs_1, Δs_2 and ΔR_1, ΔR_2, respectively. If the total sum of the valences remains constant, the following obvious condition should be fulfilled:

$$\Delta s_2 = -(\nu_1/\nu_2)\Delta s_1.$$

If we assume that $\Delta s_1 > 0$, then $\Delta R_1 < 0$ and $\Delta R_2 > 0$.

In terms of the finite differences, we have

$$\nu_1 \Delta s_1 = -(\nu_1/b)(s + \Delta s_1)\Delta R_1,$$
$$\nu_2 \Delta s_2 = -(\nu_2/b)(s + \Delta s_2)\Delta R_2.$$

Summing up the above equations, we obtain

$$\nu_1 \Delta R_1 + \nu_2 \Delta R_2 = \nu_1(\Delta s_1/s)(\Delta R_2 - \Delta R_1). \quad (9)$$

At $\Delta s_1 > 0$ and $(\Delta R_2 - \Delta R_1) > 0$, we arrive at the condition

$$\nu_1 \Delta R_1 + \nu_2 \Delta R_2 > 0.$$

This signifies that upon polyhedron distortion, the average bond length increases by the value $\Delta R_{av} = (\nu_1 \Delta R_1 + \nu_2 \Delta R_2)/n$.

Finally, let the coordination of a certain central atom be distorted in an arbitrary way, i.e., let $\Delta s_1, \Delta s_2, \ldots \Delta s_n$ be positive and $\Delta s_{n+1}, \ldots \Delta s_\nu$ be negative, so that $\sum_i^\nu \Delta s_i = 0$. Obviously, the corresponding changes in the bond lengths, i.e., $\Delta R_1, \Delta R_2, \ldots \Delta R_n$ are negative, whereas $\Delta R_{n+1}, \ldots \Delta R_\nu$ are positive. In other words, the bond lengths of the first group are reduced, whereas the bond lengths of the second group are elongated.

Thus, the average values $\Delta s_{av} = \sum_{i=1}^n \Delta s_i/n$ and $\Delta s'_{av} = \sum_{i=n+1}^\nu \Delta s_i/(\nu - n)$ obey the relationship $n\Delta s_{av} = (\nu - n)\Delta s'$ if the sum of the valences is constant.

The average change in the reduced bonds equals $\Delta R_{av} = \sum_{i=1}^n \Delta R_i/n$ and the average change in the elongated bonds equals $\Delta R'_{av} = \sum_{i=n+1}^\nu \Delta R_i/(\nu - n)$. Then, the similar reasoning leads to a conclusion that distortion results in an increase of the average bond length, i.e.,

$$[n\Delta R_{av} + (\nu - n)\Delta R'_{av}]/\nu > 0. \quad (10)$$

The distortion theorem has several corollaries:

(a) If an atom is placed into a too large void, so that the average bond length cannot satisfy the BVS equation (4), then the sum of bond valences increases because some bonds become shorter and some other ones become longer, i.e., because of the displacement of the atom from the void center accompanied by a reduction of the effective coordination number. A good example here is the high-pressure phase of magnesium silicate $MgSiO_3$ with the perovskite-like structure. A magnesium atom is too small to occupy the center of a cuboctahedral void with the coordination number 12. Therefore, the perovskite-like structure experiences strong orthorhombic distortion (a = 4.780, b = 4.933, and c = 6.902 Å), and, in fact, the magnesium atom is located in a distorted eight-vertex polyhedron.

(b) Since high pressures give rise to crystal compression, i.e., a reduction of the average bond length, an increase in the pressure reduces the distortion of the coordination polyhedron. Indeed, at higher pressures, the orthorhombic distortion of the $MgSiO_3$ "perovskite" structure becomes rather feebly marked [21].

(c) Since the nearest neighbors together with some next-nearest neighbors can always be considered as strongly distorted nearest environment characterized by a somewhat higher coordination number, an increase in the pressure would stabilize this higher coordination. Thus, the structural transformation of ilmenite (the high-pressure phase of $MgSiO_3$ with the coordination numbers of both Mg and Si being six) into the structure of distorted perovskite (with the coordination numbers of magnesium and silicon being eight and six, respectively) at higher pressures can be considered as the transition from 6 + 2 shortest bonds in the ilmenite structure to 8 shortest bonds in the orthorhombic perovskite structure. Eight shortest Mg–O bonds in the ilmenite structure range within 1.99–3.08 Å, whereas eight shortest Mg–O bonds in the perovskite structure range within a much narrower interval, 2.06–2.47 Å, thus indicating a much weaker distortion. The bond length averaged over eight shortest bonds in the ilmenite structure (2.32 Å) considerably exceeds the lengths of analogous eight bonds in the latter structure (2.21 Å), although the individual bonds in the eight-fold coordination of the perovskite-like structure are longer than the corresponding bonds in the six-fold coordination (octahedron) of the ilmenite structure.

1.3 Bond Length Correlations in Coordination Polyhedron

Upon simple transformations of the equation relating the bond valence and the bond length, one can establish the correlations or relationships between individual bond lengths in a coordination polyhedron [22]. We assume that the polyhedron is distorted in such a way that one can divide all the bonds into two groups with the bond lengths R_{ik} and R_{il}, with the numbers of bonds in each group being ν_k and ν_l ($\nu_i = \nu_k + \nu_l$), respectively. With due regard for (2) and (3), equation (1) takes the form

$$V_i = \nu_k \exp\left(\frac{R_1 - R_{ik}}{b}\right) + \nu_l \exp\left(\frac{R_1 - R_{il}}{b}\right) \quad (11)$$

or

$$V_i = \nu_k (R_{ik}/R_1)^{-N} + \nu_l (R_{il}/R_1)^{-N}. \quad (12)$$

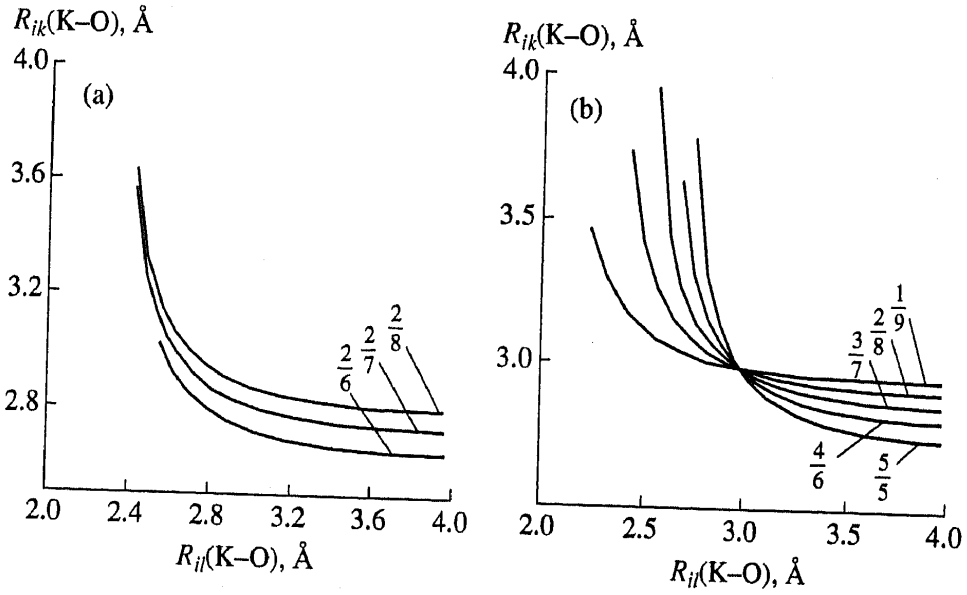

Fig. 2. Correlation between the K–O bond length at various values of the ν_k/ν_l ratios (indicated at each curve). (a) At the total coordination number ν ranging from 10 to 8; (b) at the total coordination number $\nu = 10$.

Upon some additional transformations, we have

$$R_{ik} = R_1 - b\ln\left(\frac{V_i - \nu_l\exp\left(\frac{R_1 - R_{il}}{b}\right)}{\nu_k}\right)$$

$$= R_1 + b\sum\frac{(-1)^n}{n}\left(\frac{V_i - \nu_l\exp\left(\frac{R_1 - R_{il}}{b}\right)}{\nu_k} - 1\right)^n, \quad (13)$$

$$R_{ik} = R_{il}\left(\frac{\nu_l}{\nu_k}\right)^N\left[1 - \frac{V_i}{\nu_l}\left(\frac{R_1}{R_{il}}\right)^{-N}\right]^N$$

$$= \sum_{m=0}^{\infty}\frac{N(N-1)\ldots(N-m+1)}{m!}\left(\frac{\nu_l}{\nu_k}\right)^m R_{il}^{m-N}\left(\frac{V_i}{\nu_k}\right)^{N-m}R_1^m. \quad (14)$$

The analysis of these relationships shows that the dependence of R_{ik} on R_{il} is a monotonically decreasing one and is determined by only two factors—the ratio ν_k/ν_l and the valence V_i of the atom located in the center of the coordination polyhedron (Fig. 3).

The corresponding experimental curves were constructed by Bürgi [23] for the I–I–I', S–S–S', Mo–O–Mo', and some other chains. It is seen from Fig. 4 (the I–I–I' chain) that the experimental dependences coincide with the theoretical ones calculated by equations (13) and (14).

The most often encountered distortion of the octahedral coordination of transition metal atoms is an octahedron elongated in the direction of the fourfold axis. All the bonds are divided into two axial (R_a) and four equatorial (R_e) bonds (the approximate symmetry D_{4h}). Similar experimental dependences were also studied by Gaso [24–26] and Hathaway [27]. They are well described by the model in question [22]. Figure 5 shows that the data predicted on the basis of the bond-valence method are consistent with the experimental data for another case of a distorted octahedron.

The distortion of the tetrahedral coordination was represented in the coordinates $\Delta R_k = R_{ij} - R_{ik}$, $\Delta R_l = R_{ij} - R_{il}$ with the bond angle θ [23–28]. The same data can also be represented in the ΔR_l, ΔR_k coordinates. Then, one can readily see that the dependences $\Delta R_l = f(\Delta R_k)$ describing the distortion of a tetrahedron (the approximate symmetry C_{3v}) and an octahedron (the approximate symmetry D_{4h}) are linear.

Consider the causes of such a behavior of the bond lengths. Transforming equation (11), we obtain

$$\Delta R_l = b\ln\left[1 - \frac{\nu_k}{\nu_l}\left(e^{\frac{\Delta R_k}{b}} - 1\right)\right], \quad (15)$$

where $\Delta R_k = R_{ij} - R_{ik}$ and $\Delta R_l = R_{ij} - R_{il}$. Then it becomes clear that the correlation sought is independent of the central-atom valence V_i and the unit distance R_1, but is determined, for each coordination number, only by the distortion type, i.e., by its symmetry, or, more precisely, by the ν_k/ν_l ratio.

Assuming that $\nu_l \le \nu_k$, we obtain

$$\Delta R_l \approx -\frac{\nu_k}{\nu_l}\Delta R_k. \quad (16)$$

In other words, an increment in the bond length taken with the opposite sign is proportional to the ν_k/ν_l ratio. It is seen from Fig. 6 that the experimental dependences are really linear.

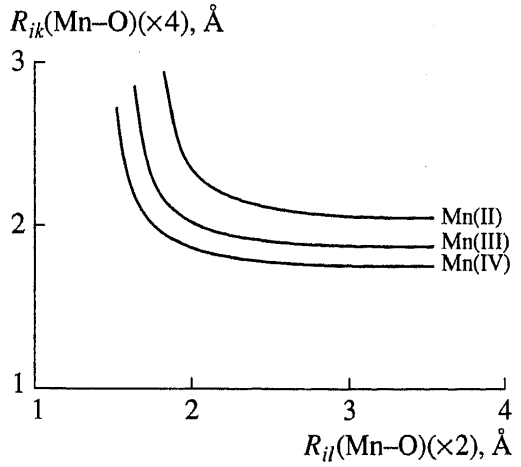

Fig. 3. Correlation between the Mn–O bond lengths at different valences of the central Mn atom (indicated at each curve), $v_k/v_l = 2/4$, $v = 6$.

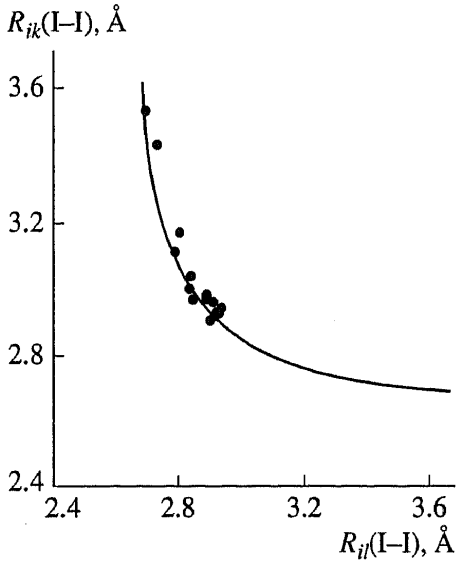

Fig. 4. Correlation of bond lengths in the I–I–I chain.

Moreover, the tangent of the slope angle of the correlation line for the octahedral coordination is set by the relationship $-v_k/v_l = -1/2$, which is quite consistent with the experimental value of the slope angle equal to –0.43. For the tetrahedral coordination, $-v_k/v_l = -1/3$, and the slope angle equals –0.30.

The variety of coordination-polyhedron distortions is not exhausted by the division of all the bonds into two groups. For the coordinations with c.n. = 6, it is often possible to distinguish three, four, and more groups of bonds with close bond lengths. In the general case, the use of the BVS equation, allows one to write the following expression

$$V_i = \sum_{n=1}^{m} v_n \exp\left(\frac{R_1 - R_{in}}{b}\right),$$

which, in turn, allows one to represent the bond length of a certain bond group as a function of bond lengths of other groups and, thus, obtain an equation analogous to (13). Such an equation provides the prediction of the distortion of coordination polyhedra with an arbitrary coordination number v_i and an arbitrary ratios of the particular coordination numbers $v_1/v_2/v_3/v_4/\ldots/v_n$.

The number of groups of bonds contained in the total coordination number determines the "dimensionality" of the data obtained. For two groups of bonds, the relation for the bond lengths can be represented by a plane curve (the two-dimensional object), for three groups, by the three-dimensional surface, etc. An example of such modeling is shown in Fig. 7.

Despite the fact that the bond-valence method successfully describes the mutual dependence of all the bond lengths in the coordination polyhedra, the fundamental causes of this phenomenon are not quite clear. Obviously, they originate from the tendency of any atomic grouping to attain the state with the minimum energy. Thus, the dependences considered above can be interpreted in terms of the potential-energy surfaces. This approach was substantiated by Boca [29] and other researchers.

1.4 Semiempirical Basis of the Model

The first energy analysis of the nature of the inverse-power dependence of the bond length on bond valence (2) was performed by Brown and Shannon [8] on the basis of the Born–Landé equation of the lattice energy of an ionic crystal

$$U(R_{ij}) = -Az_iz_j/R_{ij} + v_{ij}\beta/R_{ij}^n, \qquad (17)$$

where A is the Madelung constant, β and n are the repulsion parameters, v_{ij} is the first coordination number, and R_{ij} is the shortest interatomic distance.

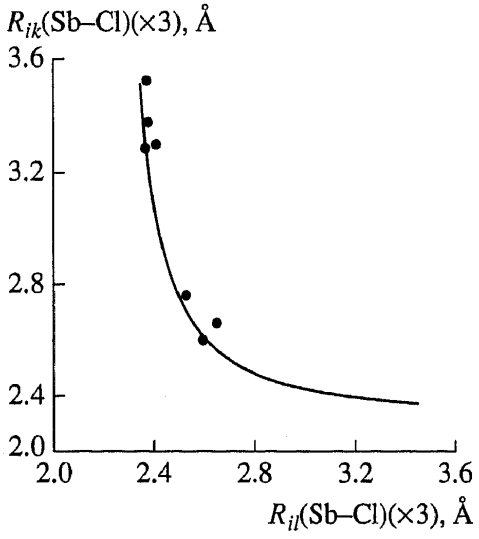

Fig. 5. Correlation of bond lengths in a distorted six-fold coordination of $SbCl_6$ ($v_k/v_l = 3/3$).

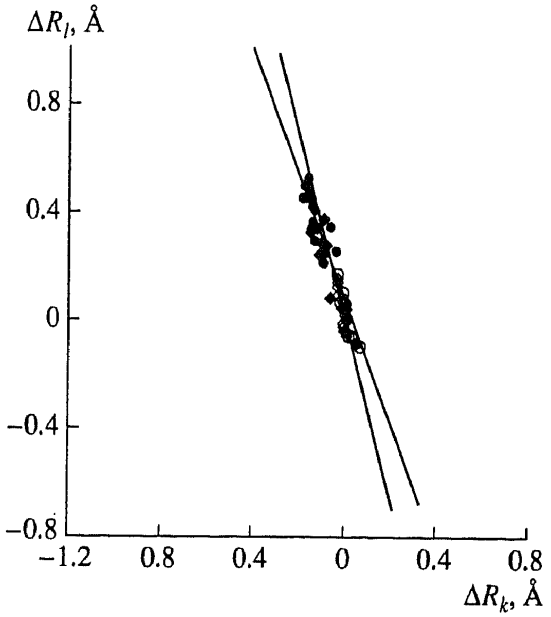

Fig. 6. Linear correlation of the increments in bond lengths during distortion of the tetrahedral and octahedral coordination. Empty squares and circles relate to $AlCl_4$ and PO_4, respectively. Dark squares and circles relate to CuF_6 and CuO_6, respectively.

Using the condition of crystal equilibrium,

$$(dU/dR)_{R_0} = 0, \tag{18}$$

where R_0 is the equilibrium value of the interatomic distance, they determined the valence of the ijth bond as

$$s_{ij} = z_i/\nu_{ij} = (\beta n/Az_j)R_{ij}^{1-n}. \tag{19}$$

For the given value of z_j and a certain structural type (A = const), one can write

$$s_{ij} = \text{const}R_{ij}^{1-n}. \tag{20}$$

For the unit bond ($s_{ij} = 1$, $R_{ij} = R_1$), we have:

$$1 = \text{const}R_1^{1-n}. \tag{21}$$

It follows from (20) and (21) that

$$s_{ij} = (R_{ij}/R_1)^{-(n-1)}. \tag{22}$$

At $N = n - 1$, the above result coincides with (2). It should be remembered that the empirical values of n (ranging within 5–12) increase with the number of electrons, i.e., with an average atomic number of the bond partners. Usually, the average n value is taken to be nine. The typical N values for a large number of oxides range from four to eight [9] and show the tendency of increasing with an increase of the atom size and the coordination number, i.e., with an increase of the average atomic number. However, the average N value ($N = 6$) is somewhat lower than it was expected ($N = n - 1 = 8$).

The exponential Born–Mayer repulsion potential,

$$U(R_{ij}) = -Az_iz_j/R_{ij} + \nu_{ij}\gamma\exp(-R_{ij}/\rho), \tag{23}$$

(where γ and ρ are the repulsion parameters) was used to substantiate equation (3) [30–32]. It was found from the equilibrium condition that $b \cong \rho(1 + 2\rho/R_1)$ [31, 32]. Indeed, the universal empirical b-value, b = 0.37 Å, somewhat exceeds the typical value of the parameter ρ for ionic crystals (0.30–0.34 Å).

Equations of type (3) were also substantiated with the aid of the modified Morse function [33], which describes the dependence of the potential energy of a covalent bond on the distance. Recently, it has been shown [31, 32] that a more complicated (combined) potential function appropriate for the bonds of the intermediate ionic–covalent nature also yields the same result. Thus, an important empirical conclusion that the bond-valence method can be applied to any chemical bond irrespectively of its nature has been proven. Ana-

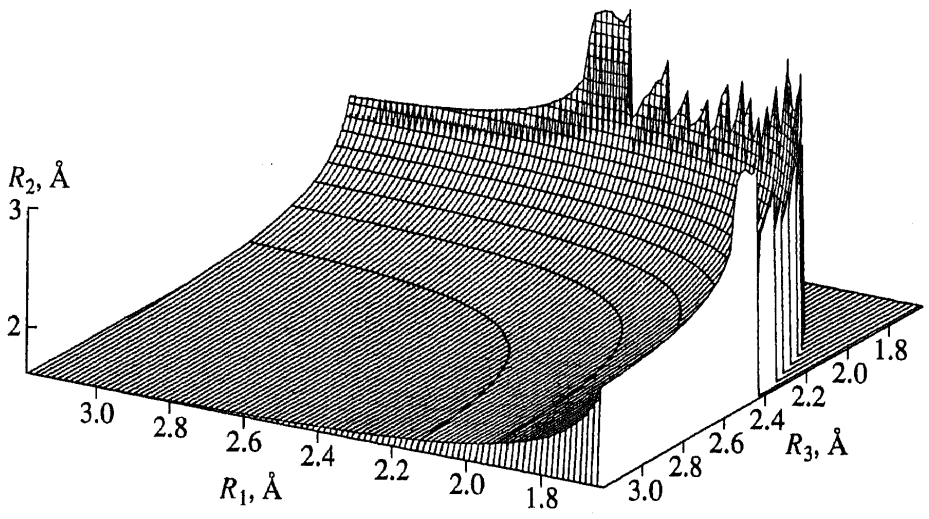

Fig. 7. Correlation of three groups of bond lengths in the distorted octahedral coordination of AlF_6: R_1 (one bond), R_2 (two bonds), and R_3 (three bonds).

lytically, the distortion theorem was proven with the use of the inverse-power dependence (2). Another important result was the confirmation of the empirical conclusion that equations (2) and (3) are almost equivalent. In particular, it was found that the unit bond lengths R_1 should be almost equal for both BVM variants and that their parameters are related as

$$N \approx R_1/b, \tag{24}$$

because

$$n - 1 \approx R_1/\rho. \tag{25}$$

The above relationships should be considered as approximate, because, strictly speaking, the parameters ρ (and therefore also b) are different for each bond and depend, in particular, on the type of the anion. This allows one to interpret the linear dependence between the experimental bond lengths R_1 [31] for the bonds formed by a large group of cations with various anions established in [17].

Finally, it was also established that the parameters R_1 are directly related to the atomic radii [31] and that they are equal to the sums of covalent radii of the bonded atoms with due regard for a certain decrease of bond lengths of purely ionic bonds. This correction is close to the empirical correction taking into account the difference between the electronegativities of bonded atoms suggested earlier in [18].

2. METHODOLOGY OF PREDICTING BOND VALENCES AND BOND LENGTHS

Prediction of bond valences and lengths with the use of the bond-valence method, the known chemical formula, and the main topological characteristics of the structure is made in several stages including: (i) the construction of the connectivity matrix describing the structure topology, and determination of bond valence sums (ii) the construction of the circuit equations, (iii) the determination of ideal bond lengths, (iv) the refinement of the details of the structure and structure mapping. Consider these stages.

2.1 Construction of the Connectivity Matrix and Determination of Bond Valence Sums

The topological characteristic of a structure can be represented in the form of the connectivity matrix. Each crystallochemical position is represented in this matrix by the type and the valence of the constituent atoms and also by all the interactions within the first coordination sphere around each atom. All the bonds for each cation form the horizontal rows, whereas those for the anions, the vertical columns of the matrix.

Consider as an example the structure of danburite $CaB_2Si_2O_8$ with the connectivity matrix in the form

	O(1) (×2)	O(2) (×2)	O(3) (×2)	O(4)	O(5)
Ca	2	2	2	0	1
B (×2)	1	1	1	0	1
Si (×2)	1	1	1	1	0

Using formula (4) and knowing the coordination of each ion, one can write the following expressions for the valence sums

$$V_{Ca} = 2s_{Ca-O(1)} + 2s_{Ca-O(2)} + 2s_{Ca-O(3)} + s_{Ca-O(5)},$$
$$V_B = s_{B-O(1)} + s_{B-O(2)} + s_{B-O(3)} + s_{B-O(5)},$$
$$V_{Si} = s_{Si-O(1)} + s_{Si-O(2)} + s_{Si-O(3)} + s_{Si-O(4)},$$
$$V_{O(1)} = 2s_{Ca-O(1)} + s_{B-O(1)} + s_{Si-O(1)},$$
$$V_{O(2)} = 2s_{Ca-O(2)} + s_{Si-O(2)} + s_{B-O(2)},$$
$$V_{O(3)} = 2s_{Ca-O(3)} + s_{Si-O(3)} + s_{B-O(3)},$$
$$V_{O(4)} = 2s_{Si-O(4)},$$
$$V_{O(5)} = 2s_{B-O(5)} + s_{Ca-O(2)}.$$

Finally, one arrives at the system of eight equations with thirteen unknowns, of which only seven are independent, because the following condition of electrical neutrality should be fulfilled:

$$2V_{O(1)} + 2V_{O(2)} + 2V_{O(3)} + V_{O(4)} + V_{O(5)} = V_{Ca} + 2V_B + 2V_{Si}. \tag{26}$$

In the general case of a crystal with n crystallochemically independent cations and m anions, the number of bonds that can have different valences is mn. The number of independent valence sums is equal to $m + n - 1$. Obviously, if $n, m > 1$, the system has no solution, because the rank of the matrix is less than the number of unknowns. The necessary equations can be obtained using the equal-valence rule (see the next section).

2.2 Construction of Circuit Equations. Equal-Valence Rule

As was indicated above, the important feature of the bond-valence method differing it from the second Pauling rule reduces to the fact that the BVM attributes a certain valence to each bond in a crystal, whereas the Pauling rule reduces to the determination of the valence strengths of cations surrounding a certain anion. In many cases, the values of the valence strength determined for both bond partners (a cation and an anion) are not equal to one another. Therefore, one arrives at the necessity of calculating a universal bond-valence value proceeding from the values of the Pauling valence strengths considered as the initial conditions. This can be made by averaging both values of the valence strength. However, in the general case, such

Table 1. Calculated and observed bond lengths in the $Ca_2B_2Si_2O_8$ structure

Bond	R_{calc}, Å	R_{obs}, Å
Ca–O(1)	2.448	2.495
Ca–O(2)	2.448	2.452
Ca–O(3)	2.448	2.466
Ca–O(5)	2.341	2.397
B–O(1)	1.489	1.481
B–O(2)	1.489	1.498
B–O(3)	1.489	1.462
B–O(5)	1.445	1.451
Si–O(1)	1.624	1.616
Si–O(2)	1.624	1.623
Si–O(3)	1.624	1.612
Si–O(4)	1.624	1.613

average values s_{ij} do not obey the valence sum rule (4). Thus, the initial Pauling values of s_{ij} should be corrected by adding some equal increments to (or subtracting them from) all the bonds of the given atom in such a way that the valence-sum rule would hold [34]. This procedure should be repeated until the s_{ij} values for all the atoms in the crystal would satisfy rule (4). Thus, the number of the fitting cycles should be approximately equal to the number of atoms in the formula unit of the crystal [34].

Schematically, the procedure of determining the individual values of the bond valences can be illustrated on a molecule of the composition *ABXY* (where *A* and *B* are cations and *X* and *Y* are anions) or on a certain hypothetical four-membered ring (also called a circuit or a loop) of the composition *A–X–B–Y* in a crystal structure. Denoting the valence of the *AX* bond by *s*, we have

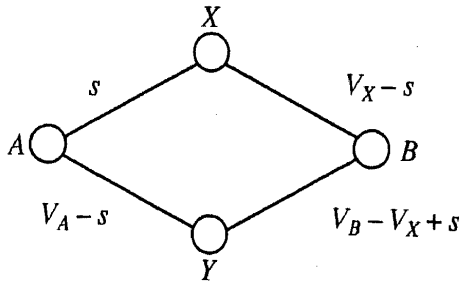

The valence of the bond calculated using the valence sum rule (4) is indicated at each segment symbolizing a bond. The differences in the bond valences at each cation are

$$\Delta s_A = s_{AX} - s_{AY} = 2s - V_A,$$
$$\Delta s_B = s_{BX} - s_{BY} = 2V_X - V_B - 2s.$$

The ring, as a whole, should satisfy the condition of the electrical neutrality, if

$$\Delta s_A - \Delta s_B = 0 \text{ (or } \Delta s_A = \Delta s_B) \text{ and}$$
$$V_A + V_B = V_X + V_Y.$$

Performing some simple transformations, we obtain

$$s_{AX} = s = (V_A/2 + q),$$
$$s_{BX} = (V_B/2 + q),$$
$$s_{BY} = (V_B/2 - q),$$
$$s_{AY} = (V_A/2 - q),$$

where $q = (V_X - V_Y)/4$.

On the other hand, the condition $\Delta s_A - \Delta s_B = 0$ can be rewritten in the form

$$s_{AX} - s_{AY} + s_{BY} - s_{AY} = 0.$$

In other words, the bond valence can be treated as a certain "vector" directed from a "cation" to an "anion." The use of the opposite direction (from an anion to a cation) changes the vector sign from plus to minus. In general, for a certain loop of bonds, the following equation is valid (with due regard for the sign alternation):

$$\sum_{loop} s_{ij} = 0. \quad (27)$$

This is the so-called the equal-valence rule (EVR) [34], which describes the tendency of bond valences of any atom in a crystal to have the values as close as possible to one another. The equal-valence rule (27) and the valence-sum rule (4) correspond to the following principle: each atom distributes its valence among all its bonds as uniformly as possible.

Brown indicates that the equal-valence rule can be used to predict the individual valences and, thus, also the bond lengths in most of the inorganic crystals [20, 34]. The only exception are the crystals in which the atom coordination is distorted by such electronic effects as the stereochemical activity of lone electron pairs and the Jahn–Teller effect for some transition metals. The special corrections to this rule should also be introduced in the case of steric hindrances (as in the case of symmetry lowering in the perovskite-like structures).

Another method for predicting individual bond valences based on the Pauling principle of the electrical neutrality of the crystal was suggested by Baur [5]. This method is also consistent with the method of bond-valence sums (4) and yields similar results.

With due regard for all the above stated, the system of seven BVS equations for danburite can be complemented with five EVR equations to form the system sufficient for determining 12 unknown bond valences:

$$s_{Ca-O(1)} - s_{Ca-O(2)} + s_{B-O(2)} - s_{B-O(1)} = 0,$$
$$s_{Ca-O(2)} - s_{Ca-O(3)} + s_{B-O(3)} - s_{B-O(2)} = 0,$$

$$s_{Ca-O(3)} - s_{Ca-O(5)} + s_{B-O(5)} - s_{B-O(3)} = 0,$$

$$s_{B-O(1)} - s_{B-O(2)} + s_{Si-O(2)} - s_{Si-O(1)} = 0,$$

$$s_{B-O(2)} - s_{B-O(2)} + s_{Si-O(1)} - s_{Si-O(2)} = 0.$$

The matrix form of the structure topology describes closed circuits whose vertices are formed by the corresponding bond valences. Therefore the equations received the name of the circuit equations.

Now, with due regard for the above stated, one can solve the system of equations. Writing the system of equations in the complete form, we arrive at the following basic matrix

$s_{Ca-O(1)}$	$s_{Ca-O(2)}$	$s_{Ca-O(3)}$	$s_{Ca-O(5)}$	$s_{B-O(1)}$	$s_{B-O(2)}$	$s_{B-O(3)}$	$s_{B-O(5)}$	$s_{Si-O(1)}$	$s_{Si-O(2)}$	$s_{Si-O(3)}$	$s_{Si-O(4)}$	B
2	2	2	1	0	0	0	0	0	0	0	0	2
0	0	0	0	1	1	1	1	0	0	0	0	3
0	0	0	0	0	0	0	0	1	1	1	1	4
1	0	0	0	1	0	0	0	1	0	0	0	2
0	2	0	0	0	1	0	0	0	1	0	0	2
0	0	1	0	0	0	1	0	0	0	1	0	2
0	0	0	0	0	0	0	0	0	0	0	2	2
0	0	0	0	0	0	0	2	0	0	0	0	2
1	−1	0	0	−1	1	0	0	0	0	0	0	0
0	0	1	−1	0	0	−1	1	0	0	0	0	0
0	1	−1	0	0	−1	1	0	0	0	0	0	0
0	0	0	0	1	−1	0	0	−1	1	0	0	0
0	0	0	0	0	1	−1	0	0	−1	1	0	0

Here B is a constant term of the equation equal to the valence of the atom for which the BVS equation is written. The last five rows of the matrix correspond to the circuit equations.

The above matrix yields the following bond valences for the structure:

$$s_{Ca-O(1)} = 0.238, \quad s_{Ca-O(2)} = 0.238,$$
$$s_{Ca-O(3)} = 0.238, \quad s_{Ca-O(4)} = 0, \quad s_{Ca-O(5)} = 0.331,$$
$$s_{B-O(1)} = 0.741, \quad s_{B-O(2)} = 0.741,$$
$$s_{B-O(3)} = 0.741, \quad s_{B-O(4)} = 0, \quad s_{B-O(5)} = 0.834,$$
$$s_{Si-O(1)} = 1.020, \quad s_{Si-O(2)} = 1.020,$$
$$s_{Si-O(3)} = 1.020, \quad s_{Si-O(4)} = 1, \quad s_{Si-O(5)} = 0.$$

The bond lengths corresponding to these bond valences can be obtained from (2) and (3). Their values are listed in Table 1 together with the corresponding experimental bond lengths determined in [35].

Some other examples of the bond lengths calculated by the bond-valence method are considered in Appendix 2.

2.3 Introduction of Weight Factors

Earlier [10], it was shown that in some cases, the introduction of weight factors (ideal values of the valence strengths of atoms, according to the initial Pauling scheme) into the circuit equations can make the calculated values closer to the experimental data.

The weight factors "refine" the contribution made by each element of the connectivity matrix to its solution, which allows a more uniform (more symmetric) valence distribution, i.e., makes the coordination polyhedron as close as possible to its ideal shape.

To illustrate the introduction of weight factors, consider the matrix of the type

	X	Y	Z
A	s_{AX}	s_{AY}	0
B	s_{BX}	0	s_{BZ}
C	0	s_{CY}	s_{CZ}

for which the equation of the six-membered loop has the form

$$s_{AX} - s_{AY} + s_{CY} - s_{CZ} + s_{BZ} - s_{BX} = 0. \qquad (28)$$

If the valences of the atoms A, B, and C, and therefore also the their bond valences s_A, s_B, and s_C are different, one has to introduce the weight factors to the loop equation. We considered several variants of such weight factors. The best weight factors were those proportional to the Pauling bond strengths of those ions

Table 2. Calculated and observed structural parameters for the rutile structure

Structural parameter, Å	Calculated	Observed
a	(4.584)	4.584
c	(2.953)	2.953
Ti–O (×4)	1.942	1.945
Ti–O (×2)	1.975	1.975
$O–O_{min}$	2.524	2.532

Table 3. Calculated and observed structural parameters for the brookite structure

Structure parameter, Å	Calculated	Observed
a	(9.184)	9.184
b	(5.447)	5.447
c	(5.145)	5.145
Ti–O(1)	1.888	1.865
Ti–O(1')	2.017	1.992
Ti–O(1")	1.977	1.994
Ti–O(2)	1.933	1.919
Ti–O(2')	1.925	1.946
Ti–O(2")	2.025	2.039
$O(1)–O(1)_{min}$	2.511	2.485
$O(2)–O(2)_{min}$	2.534	2.514

Table 4. Calculated and observed structural parameters for the anatase structure

Structural parameter, Å	Calculated	Observed
a	(3.785)	3.785
c	(9.514)	9.514
u(O)	0.2114	0.2066
Ti–O (×4)	1.928	1.937
Ti–O (×2)	2.011	1.966
$O–O_{min}$	2.507	2.448

that provided the maximum difference in valences (usually, these were cations):

$$(s_{AX} - s_{AY})/s_A + (s_{CY} - s_{CZ})/s_C + (s_{BZ} - s_{BX})/s_B = 0. \quad (29)$$

In most of the instances, the use of the above weighting scheme provides the construction of a more accurate model. Thus, the introduction of the weight factors for the $Y_2SiBe_2O_7$ compound with the melilite-type structure, reduced the mean-square deviations of the bond lengths from their experimental values from 0.026 Å to 0.021 Å [36].

If a compound consists of atoms with considerably different valences (e.g., uni- and pentavalent cations), the direct solution of the system of linear equations can yield negative (i.e., physically senseless) valences for the weakest bonds. The use of the weighting scheme allows one to avoid similar situations.

Below, we consider the corresponding calculations for the KVO_3 structure first solved by Rutherford [37]. The structure contains two uni- and pentavalent cations, and therefore the use of the conventional methods yielded the negative bond valences. The introduction of the weight factors for cations eliminated this difficulty and increased the accuracy of the model. Both variants of the calculated bond valences and the corresponding experimental data [37] are indicated below.

Bond	s_{ij} without weights	s_{ij} with weights	s_{ij} obs. [37]
K–O(1)	–0.115	0.061	0.150
K–O(2)	0.154	0.110	1.165
V–O(1)	1.115	0.939	0.950
V–O(2)	1.385	1.560	1.490

2.4 Refinement of Crystal Structures. Mapping of Bond Valences

Upon the determination of "ideal" interatomic distances and atomic coordinates by the bond-valence method, the results obtained can be refined using the distance least-squares (DLS) method [38] based on the least-squares procedure for the search of the minimum value of the functional

$$\Delta R = \sum_j \omega_{ij}^2 (R_{ij} - R_{ij}^0)^2, \quad (30)$$

where R_{ij}^0 is the standard interatomic distance and ω_{ij} is the weight factor.

At this stage, it can also be necessary to take into account next nearest neighbors forming no direct bonds with the atom under question and the corresponding bond angles. This would provide the minimization of repulsion between the atoms or ions not bound directly. This approach provides the prediction of bond lengths within an error less than 0.05 Å if no considerable electron and steric distortions take place [20]. The further refinement of the crystal structure can be performed by several methods. One of them was suggested by Walterson [39] in order to localize lithium atoms in lithium tungstates. The method reduces to the calculation of the sum of bond valences which would have been possessed by a Li atom placed at a certain arbitrary point of the crystal space. The positions in which this sum would have been close or equal to the unit valence, are recognized as probable location of lithium atoms. If the sum of the valences exceeds unity, the

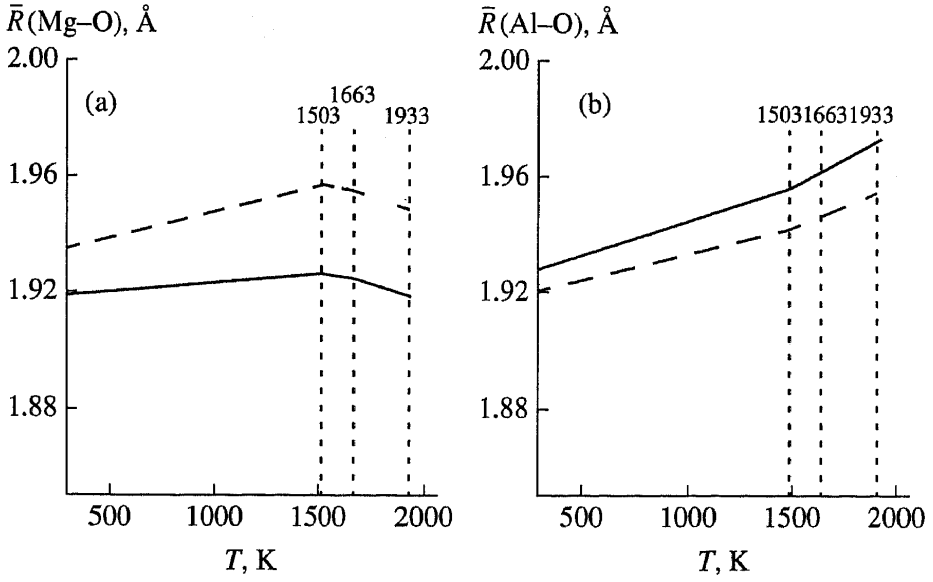

Fig. 8. Interatomic distances in the spinel structure calculated by the VLS method at various temperatures and the corresponding experimental data: (a) the Mg–O distance, (b) the Al–O distance.

Li–O distances would be too short; if this sum is less than unity, the distance would be too long. Varying consistently the positions of lithium atoms, Walterson managed to construct the map of valence sums, which revealed all the possible positions for lithium atoms. In addition to localization of individual atoms of the structure, the valence-sum map also provides the determination of all the empty cavities in the structure along which the atomic transport (in particular atomic diffusion) can proceed.

A very convenient method of valence-sum mapping was suggested by Brown [40]. He used the function

$$f = \left(\sum_j s_{ij}/V_i\right)^{-n}, \qquad (31)$$

with the exponent n arbitrarily chosen in the range from 8 to 16.

The maps constructed with the use of this function show sharp maxima at the points where the valence-sum maps show minima, i.e., at the voids of the structure. The values of the peaks drastically decrease along the directions, where the valence sums increase. The ideal position of the ith atom with valence V_i corresponds to $f = 1.0$. Applying this method to the forsterite structure Mg_2SiO_4, Brown managed to determine the positions of Mg(1) and Mg(2) atoms and also possible paths of Mg(1) diffusion. It looks like that the Mg(2) atoms "cannot find" appropriate diffusion paths.

Earlier [38], our group suggested to minimize the deviations from the experimentally determined valence in modeling crystal structures by the so-called valence least-squares (VLS) method. Using the least-squares procedure, we minimized the following differences

$$\Delta V = \sum_i \omega_i^0 (V_i - \sum s_{ij})^2, \qquad (32)$$

where V_i is the formal valence of the ith atoms and ω_i is a certain weight factor.

This functional was tested on the rutile TiO_2 structure. It was shown that it is possible to attain an almost zero value of this functional, $\Delta V = 0$, for any set of the unit-cell parameters a and c. For instance, using certain unit-cell parameters, $a = 4.22$ Å and $c = 3.38$ Å, we arrived at a conclusion that the TiO_2 structure with these parameters consists of regular TiO_6 octahedra with the Ti–O distances 1.97 Å and the oxygen coordinate $x_0 = 0.38$. Thus, it is clear that the minimization of functional (32) should be performed at the experimen-

Table 5. Interatomic distances in the spinel structure calculated by the VLS method at various temperatures and the corresponding observed values [42]

T, K	R(Mg–O)$_{VLS}$, Å	R(Mg–O)$_{obs}$, Å	R(Al–O)$_{VLS}$, Å	R(Al–O)$_{obs}$, Å
293	1.9349	1.9188	1.9201	1.9273
1503	1.9566	1.926	1.9416	1.9562
1663	1.955	1.9242	1.9464	1.9627
1933	1.9488	1.9183	1.9553	1.9733

tal unit-cell values in such a way that only free atomic coordinates are varied. For rutile, these were the coordinates x of the oxygen position $(x, x, 0)$. Irrespectively of the choice of the initial x_0 values (ranging from 0.25 to 0.40), the calculated value of this coordinate is $x_0 = 0.3053$, which agrees quite well with its experimental value $x_0 = 0.3050(3)$. Tables 2–4 list the results of similar modeling and the corresponding experimental values for the rutile, brookite, and anatase structures.

However, the experience of the VLS refinement of more complicated structures (e.g., of kyanite Al_2SiO_5) showed that satisfactory results are obtained only if the initial coordinates differ from the true ones by not more than 0.025. In such cases, one has, first, to determine the initial coordinates by the DLS method and then use these coordinates in the further refinement.

One can successfully use as a standard (ideal) distance the distance predicted by the bond-valence method. The further refinement of the model is made by the VLS method. Such a combined procedure is called the distance valence least-squares (DVLS) method [38]. This method was successfully used for modeling the spinel structure $MgAl_2O_4$ (sp. gr. $Fd3m$) [41]. In order to determine the parameter a of the cubic unit cell and the coordinates (u, u, u) of oxygen atoms, the values of these parameters were varied within the ranges $7.5 < a < 8.5$ Å and $0.35 < u < 0.40$, respectively. The values of the bond valences s_{ij} in the functional (32) were set using equation (2) of the bond-valence method. Moreover, thermal expansion of the bonds was also taken into account using the formula

$$R_1(T) = R_1(1 + \alpha\Delta T),$$

where α is the linear expansion coefficient of the bonds equal to $\alpha(Mg–O) = 1.2 \times 10^{-5}$ deg^{-1} and $\alpha(Al–O) = 1.1 \times 10^{-5}$ deg^{-1} [42]. DVLS-modeling was performed at the temperatures 293, 1503, 1663, and 1933 K, at which the precision X-ray data are known [42].

Table 5 and Fig. 8 illustrate the results of DVLS-modeling for spinel and show satisfactory agreement between the model and the experiment. The interatomic distances calculated at different temperatures agree with the experimental dependences $R(T)$ (Fig. 8), although it was assumed [42] that partial spinel inversion (disordering of Mg and Al atoms) could take place at $T > 1503$ K. However, modeling performed show that such an assumption is not necessary.

3. APPLICATIONS OF THE BOND-VALENCE MODEL

3.1 Valence-Matching Principle

As is well known [43], the formation of stable compounds, including crystalline ones, obeys the general rule known as the principle of hard and soft acids and bases (HSAB principle), which states that stable products of any reaction consist of the combinations of a hard (Lewis) acid with a hard base and a soft acid with a soft base:

$$(HA)(SB) + (SA)(HB) \longrightarrow (HA)(HB) + (SA)(SB).$$

The hardness and the softness of acids and bases have not been quantitatively characterized as yet. Pearson [43] divided acids and bases into three groups—hard, soft, and intermediate. A more detailed systematization can be made if one takes into account the geometrical characteristics of atoms and ions (their radii), polarizabilities, electronegativities, etc. [44]. Recently, Brown suggested to use the characteristic bond valence $\langle s \rangle$ of bonds formed by an anion or a cation under study [45]:

$$\begin{aligned} s_k &= \langle s \rangle_k = V_k/\langle \nu \rangle, \quad V_k > 0, \\ s_a &= \langle s \rangle_a = V_a/\langle \nu \rangle, \quad V_a < 0, \end{aligned} \tag{33}$$

where $\langle \nu \rangle$ is the average coordination number of the cation or the anion obtained by the statistical processing of a large set of experimental data [45]. It was shown [46] that the thus obtained s_k values correlate with the electronegativity of many cations.

Since anions form bonds in a larger range of valences than cations, it is expedient to define the maximum strength of a base as

$$s_{max} = V/\nu_{min}. \tag{34}$$

Here ν_{min} is the minimum coordination number of an anion.

The valence-matching principle (VMP) states that the stable compounds are formed by Lewis acids and bases with close values of the characteristic bond valences and are not formed otherwise [46].

The HSAB principle was tested on numerous silicates, phosphates, and other groups of substances [44]. It was found that monovalent alkali metals (soft acids) cannot form orthosilicates having island-type structures, whereas the high-valence cations (Zr^{4+}, Ti^{4+}, Al^{3+}, etc.) (hard acids) cannot form polymerized silicates. Later, a similar conclusion was also drawn in [47].

The direct comparison of valence characteristics of acidity and alkalinity of atoms playing various crystallochemical roles makes the basis of the notion of a "mineralogically probable structure", i.e., a crystal structure that can be formed, with a high probability, in the crystallization process under the natural conditions [48]. The examples are the silicates with the general formula $A_mSi_nO_p$ [48, 49], where A are the large (with the radii exceeding 1 Å) monovalent cations such as Na^+, K^+, Rb^+, and Cs^+. It was shown that numerous synthesized compounds of such type relate to the group of mineralogically improbable compounds. The stability of such structures decreases with a decrease of the polymerization degree of SiO_4-tetrahedra and an increase of the A^+-cationic radii, so that the orthosilicate with the formula Cs_4SiO_4 should be the least stable compound. For the fulfillment of the local valence balance (the bond-valence matching) in the hypothetical

structure of the latter compound, each oxygen atom should be bonded to one Si-atom and four Cs^+-ions displaying an unplausibble fourfold coordination.

The combination of the valence-matching principle and the bond-valence sum rule (4) can be efficiently used, e.g., in the analysis of stable configurations of the short-range order in the distribution of heterovalent atoms among the crystallographically nonequivalent positions. Such a procedure was recently used [50] in the determination of the most probable location of cations in complicated monoclinic calcium, sodium–calcium, and alkali amphiboles, in which the heterovalent substitutions occur over several crystallographically nonequivalent positions: the large cavities *A* inside double hexagonal rings of (Al, Si)-tetrahedra (the Na^+, Ca^{2+}, vacancy), four octahedral, *M*(1), *M*(2), *M*(3), *M*(4) positions (*M* = Li^+, Mg^{2+}, Mn^{2+}, Mn^{3+}, Al^{3+}), and two tetrahedral, *T*(1) and *T*(2), positions (*T* = Al^{3+}, Si^{4+}). This analysis showed that only some (usually, not more than three or four) configurations of cations from the neighboring positions can simultaneously meet both VMP and BVS requirements.

The maximum number of such configurations is determined in the pargasite, $NaCa_2(Mg_4Al)[Si_6Al_2O_{22}](OH)_2$, structure. The condition of the minimum deviation of the bond-valence sum from the formal valences of the cations and anions admits four variants of the short-range order:

	M(1)	*M*(2)	*M*(3)	*M*(4)	*A*	*T*(1)	*T*(2)
(I)	Mg	Al	Mg	Ca	Na	Al	Si
(II)	Mg	Mg	Mg	Ca	–	Si	Si
(III)	Mg	Mg	Al	Ca	Na	Al	Si
(IV)	Mg	Mg	Al	Ca	–	Si	Si

The local compensation of the valences is attained due to the fact that the Al atoms located in the octahedral *M*(2) and *M*(3) positions are the neighbors of the Al atoms occupying the tetrahedral *T*(1) position. Moreover, the additional contributions to the valences of the oxygen atoms coordinating aluminum come from the Na atoms in the *A* positions. If both types of the tetrahedra are occupied by Si atoms, the more favorable situation is the location of Mg in the *M*(2) position and the formation of vacancy in the *A* position.

The neighboring regions (I, II, III, and IV) characterized by various types of the short-range order can be "placed" into the crystal structure because of a certain bond-length relaxation at the boundaries between these regions. The diffraction methods can reveal only the configuration averaged over all the regions with various types of the short-range order (the so-called average structure). However, the appropriate interpretation of the IR, NMR, NGR, EXAFS, etc. spectroscopic data requires the knowledge of the short-range order.

3.2 Evaluation of Atom Valence from Structural Data

This classical problem solved by the BVM is, in fact, inverse to the prediction of interatomic distances, i.e., equation (4) is solved with respect to V_i at the known distances R_{ij}. This problem arises if, by any reason, the valence of one or several atoms in the structure is unknown or if the structure contains atoms in different valence states. For example, the valence sum close to unity in the oxygen position indicates the probable presence in the close vicinity of a hydrogen atom, i.e., the existence of the hydroxyl group OH^-. It is especially difficult to localize hydrogen in structures containing heavy atoms. In these cases, modeling with the calculation of bond valences can indicate the most probable location of hydrogen bonds. Recently, such modeling was performed for the carminite structure, $PbFe_2(AsO_4)_2(OH)_2$ [51].

The positions of O^{2-} and F^- ions can be distinguished even if the numbers of electrons and interatomic distances in both cases are rather close, i.e., if the X-ray diffraction data do not allow the identification of the kinds of atoms. An example is the LaOF structure [52]. The La^{3+} cation in this structure is surrounded with four O^{2-} and four F^- ions. Taking into account the values of the ionic radii, the longer interatomic distances (2.60 Å) should be attributed to the La–O bonds, whereas the shorter ones (2.42 Å), to the La–F bonds, as was made by Zachariasen in the early determination of this structure [12]. However, the calculation of the corresponding bond valences (s = 1/2 for La–O and s = 1/4 for La–F) show that in fact, La–F bonds are longer than La–O bonds, which is confirmed by the recent X-ray study of this structure.

The specific problem solvable by the bond-valence method is the determination of the individual valences of atoms occupying crystallographically nonequivalent positions. This problem can be successfully solved, e.g., for Cu^I, Cu^{II}, and Cu^{III} atoms in structures of high-temperature superconductors [53].

In some cases, the calculation of experimental bond-valence sums indicates the presence of atoms in mixed valence states in the nonequivalent positions of the structure. Thus, valences of V atoms occupying four crystallographically nonequivalent positions in the V_4O_7 structure calculated from the measured interatomic distances lie within 3.3–3.6 v.u., with the average value being 3.48 v.u. (the average valence for the stoichiometric composition is 3.50 v.u.) [10].

Numerous precision experimental data on the nearest neighbors and bond lengths of individual atoms have been obtained recently for crystalline substances, isolated molecules and molecules and ions in solutions by various X-ray spectroscopy methods (XAS, EXAFS, and XANES). In these cases, one has to determine several valences of atoms of a certain chemical element located in different positions of the structure.

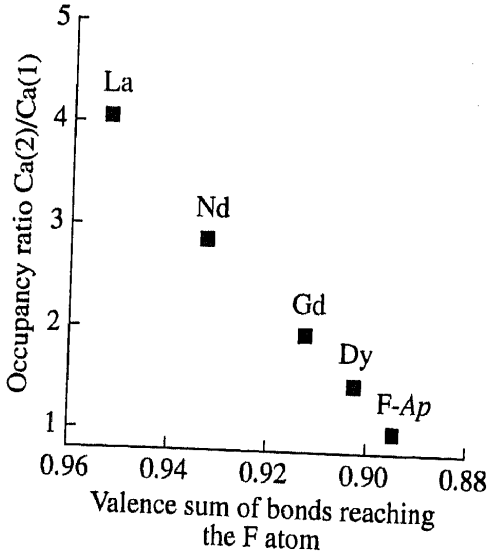

Fig. 9. Correlation between the occupancy ratio Ca(2)/Ca(1) for positions Ca(2) and Ca(1) occupied by rare earth atoms and the valence sums for the bonds reaching the F atom in the apatite structure.

This can be made by calculating the bond-valence sums (4) for individual atomic positions. This method was used to determine the states of metal oxidation in metalloproteins and other organometallic complexes [54–59].

3.3 Positional Preference in Heterovalent Solid Solutions

In a number of studies on the structural ordering in synthetic F- and OH-apatites containing various impurities performed in the early seventies [60, 61], it has been established that rare earth elements usually substitute Ca in the position Ca(2) (a seven-vertex polyhedron with F or OH at one of the vertices, the symmetry C_s) and not the Ca(1) position (a nine-vertex polyhedron—the tricapped trigonal prism, the symmetry C_3). This results in a situation paradoxical in terms of ionic sizes—the larger light TR^{3+} (La^{3+}, Nd^{3+}) ions show the tendency to occupy a smaller seven-vertex polyhedron of Ca(1) and not a larger nine-vertex polyhedron of Ca(2). Later, these experimental observations were repeatedly confirmed by X-ray determinations of both natural [62] and synthesized [63] fluorapatite single crystals.

These facts were first interpreted upon the detailed analysis of the energy effects of ordering [64]. The calculations of the crystal energy showed that the electrostatic potential in the position Ca(2) is 4% higher than the potential in the position Ca(1). This explains the tendency of impurities with the charge exceeding the charge of Ca^{2+} to occupy the Ca(2) position. These are the impurities of trivalent and those bivalent atoms that have lower electronegativities (Sr^{2+} and Ba^{2+}). These results are inconsistent with the predictions based on a simple geometric model, according to which the larger atoms should occupy the Ca(1) position.

Later, it was discovered [62, 63] that in the fluorapatite (F-*Ap*) structure, the Ca(2) and, especially, the F atoms coordinating Ca(2) have "undersaturated" bond-valence sums (1.88 and 0.89, respectively). The partial substitution of Ca by a trivalent atom in the position Ca(2) levels the bond-valence sums in the positions Ca(1) and Ca(2) and decreases the valence undersaturation of the fluorine atom. It was shown [63] that there is the inverse correlation between the occupancies of the positions Ca(2) and Ca(1) with rare earth atoms and the valences of the bonds reaching the F-ion (Fig. 9).

It is seen from Fig. 9 that the occupancy ratio Ca(2)/Ca(1) rapidly decreases with the transition from large light TR^{3+} ions to small heavy ones. This signifies that the efficiency of rare earth atoms compensating the valence undersaturation of F atom decreases with a decrease of the atomic number. It seems to be associated with the fact that the interatomic Ca(2)–F distance is not decreased with a decrease of the radius of the TR^{3+} ion in the position Ca(2), but even slightly increases (from the value 2.310 Å in La–F-*Ap* up to 2.314 Å in Dy–F-*Ap*) [63].

Recently, it was assumed [65] that the criterion of valence undersaturation in one or several Ca positions in a number of Ca-containing minerals can indicate the preferential occupancy of these positions by highly charged (in particular, rare earth) atoms. Thus, the calculations showed that the Ca–O bonds in the Ca(2) position in the minerals of the clinozoisite–epidote group are considerably longer (on the average, by 0.1 Å) than in the Ca(1) position and that the total bond valence of the Ca(2) position equals 1.7 instead of 2.0 for the Ca(1) position. Indeed, the refinement of the structures of rare earth-containing minerals of this groups (allanite, dissakisite, and dollaseite) confirms that the rare earth atoms are preferably located in the position Ca(2). In a similar way, of four Ca positions in vesuvian, three are valence-supersaturated and only the position Ca(3) is noticeably undersaturated. The refinement of this structure showed that the rare earth impurities tend to substitute Ca in the Ca(3) position.

The structure of the rare mineral cuspidine, $Ca_4[Si_2O_7]F_2$, has four crystallographically nonequivalent Ca positions of which two, Ca(3) and Ca(4), are "less saturated" with the Ca–O and Ca–F bond valences than two other positions, Ca(1) and Ca(2). The recent structural refinement of cuspidine [63] showed that the rare earth atoms preferably enter the first pair of the positions, thus increasing the total valence of the bonds in those positions.

3.4 Bond Valence and Crystal Properties. Correlation Between Thermal Expansion and Compressibility and the Bond-Valence Gradients

Both energy of molecule dissociation (atomization of a crystal) and the bond valence depend on the interatomic distances in a similar way—according to the exponential or inverse-power laws. Therefore one can expect that the relation between these quantities would be rather simple, probably even linear. Indeed, it was shown [66] that the relation between the dissociation energy E(C–O) of the C–O bonds and their valences is of a simple linear form approximately described by the equation

$$E(\text{C–O}) \cong Js,$$

where $J = 96$ kcal/(mol v.u.). The assumption about the linear character of the above dependence was extended to inorganic crystals [67]. The parameters J were calculated for several dozens of cation–oxygen bonds.

The above hypotheses can be verified by independent methods on the substances whose polymorphic modifications include the atoms with various coordination numbers, e.g., on three polymorphs of Al_2SiO_5—sillimanite, andalusite, and kyanite. One of the Al atoms has the same coordination number (six) in all the polymorphs, whereas another aluminum atom is in a tetrahedron (c.n. = 4), five-vertex polyhedron (c.n. = 5), and an octahedron (c.n. = 6), respectively. Thus, the average bond valences of the Al–O bonds in these polymorphs are 5/8, 11/20, and 1/2, respectively. Figure 10 shows the dependence of E on s.

In some cases, the thermal expansion coefficients and the bond valences showed some correlation. The bond-valence maps obtained for atoms displaced from their equilibrium positions toward neighboring atomic positions calculated for three Al_2SiO_5 polymorphs (kyanite, sillimanite, andalusite) [38] are shown in Fig. 11. The isolines are elongated along the directions where the s gradient with respect to the atomic coordinates is minimal. It seems that these directions should coincide with the directions of atomic-coordinate variations with an increase (decrease) in the pressure and temperature. Indeed, the arrows in Fig. 11 indicate the directions of the changes of the atomic coordinates in the andalusite structure observed with an increase of the pressure and temperature, which almost coincide with the direction of isoline elongation. It is seen that, under the action of high pressures and high temperatures, atoms are displaced in the opposite directions.

Table 6 lists the experimental changes in the bond lengths [68], the corresponding thermal expansion coefficients in the andalusite structure, and the corresponding calculated changes in the bond valence in the temperature range from 25 to 1000°C. One can see an obvious inverse correlation between these properties—the bond length varies the more pronouncedly, the less is the change in the bond valence.

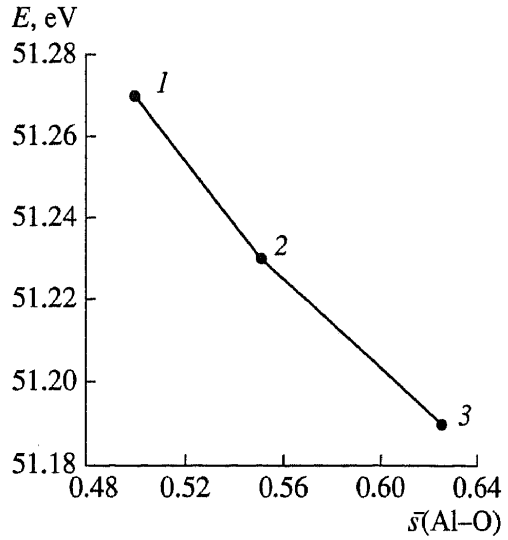

Fig. 10. Correlation between the atomization energy E and the average valence s of the Al–O bonds in three Al_2SiO_5 polymorphs: (*1*) sillimanite, (*2*) andalusite, (*3*) kyanite.

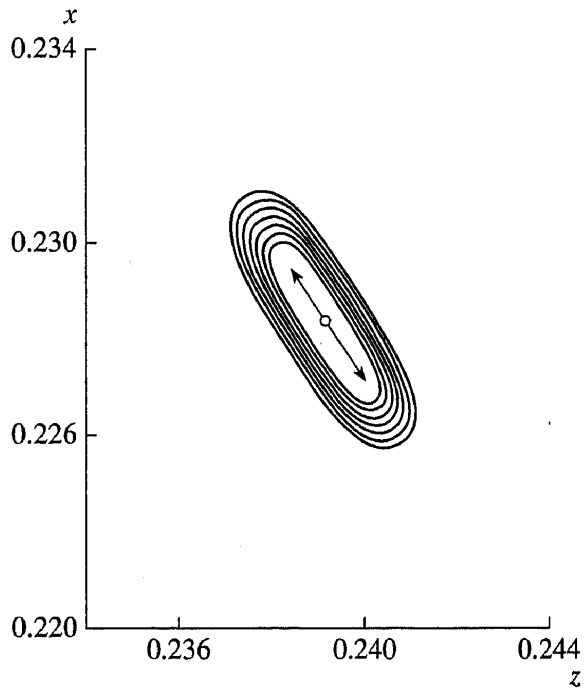

Fig. 11. Isolines of bond valence as a function of the x and z coordinates of the O_d atom in the andalusite structure. The circle in the center indicates the equilibrium position of the O_d atom. The isolines are spaced by 0.005 v.u.

Recently, Brown *et al.* [69] managed to predict thermal variation of bond lengths in terms of the bond valence method, in particular, using the distortion theorem. Let an atom be symmetrically surrounded with its neighbors and perform thermal vibrations with the amplitude δR around its center, so that the instantaneous bond-length value obeys the relationship

$$R' = \langle R \rangle + \delta R,$$

where $\langle R \rangle$ is the time-averaged bond length and δR

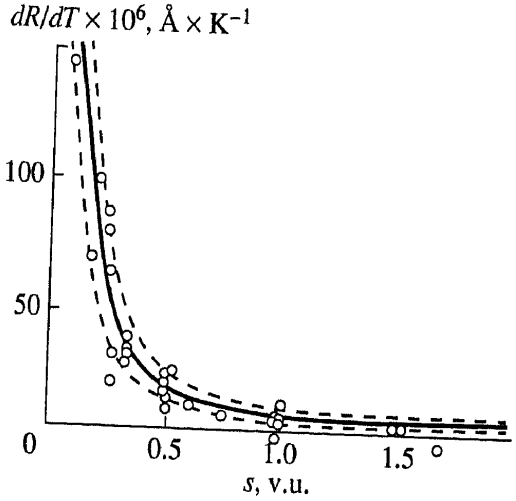

Fig. 12. Correlation between the temperature variation of the bond length averaged over all the cations $\langle dR/dT \rangle$ and the bond valence s.

changes with time in such a way that its average value is zero. Expanding equation (3) of the instantaneous bond length into a series,

$$s' = \exp((R_0 - R')/b) = \exp((R_0 - \langle R \rangle)/b) \times \exp(\delta R/b) = \exp((R_0 - \langle R \rangle)/b) \times [1 - \delta R/b + \delta R^2/2b^2 + \ldots]$$

and ignoring the terms of orders higher than second, we obtain

$$\Delta R = \langle \delta R^2 \rangle / 2b,$$

where $\Delta R = \langle R \rangle - R_e$, R_e is the bond length in the absence of thermal vibrations. Substituting the constant $b = 0.37$ Å into the above equation and introducing the notation $U = \langle \delta R^2 \rangle$, we obtain

$$\Delta R = 1.35U.$$

Thus, the thermal elongation of the bond length is proportional to the mean-square deviation of the bond length from its average value. Differentiating both sides of the equation, we have

$$dR/dT = d\Delta R/dT = 1.35(dU/dT).$$

The above equation can also be written in the form

$$dR/dT = 1.35k/G,$$

where k is the Boltzmann constant. The force constant G can be described by the following expression relating it to the bond valence s:

$$G = cs - d(1 - \exp(-cs/d)),$$

where c and d are the empirical constants.

Figure 12 illustrates the good agreement of the model with the experimental data taken from the ICSD.

3.5 Analysis of Geometric Strains and Electronic Effects in Crystal Structures

As has already been indicated, the methodology considered above provides the determination of an idealized scheme of the bond-valence distribution in a crystal structure with the known chemical composition and topology. This methodology allows one to indicate only the number and the formal valence of the nearest neighbors. It is clear that such a description of the structure is far from being complete, because it contains no information about the structure symmetry. Therefore the calculated bond valences and the corresponding interatomic distances (upon the introduction of corrections for electronic effects) are called "simple" or "ideal" [14]. However, the term "unstrained-bond valence" seems to be more preferable, because it corresponds to the condition of the highest symmetry of the bond distribution for the given crystal topology. Therefore, the comparison of the theoretically predicted and experimentally determined bond lengths can be used in the search for most strained regions in the structure (which can simultaneously be the sites of the highest reactivity or lability) and in the search for strains of the structure as a whole. The latter requires the development of the criteria of the structure stability in terms of the geometric strains caused by the so-called nonlocal steric hindrances [14].[1]

Consider the advantages provided by such an analysis on several examples. It is well known that the oliv-

[1] The well known example of local steric effects is a hydrogen bond [14]. Usually, a small hydrogen atom is located in a too large void and therefore forms nonsymmetric bonds.

Table 6. Changes in the cation–anion bond lengths in andalusite during heating from 25 to 1000°C and the corresponding bond-valence gradient

Distance	Change in bond length, Å	Thermal expansion coefficient of bond, deg^{-1}	Bond-valence gradient
Al(1)–O_a	4×10^{-3}	2.2×10^{-6}	0.0069
Al(1)–O_b	2×10^{-3}	1.1×10^{-6}	0.0058
Al(1)–O_d	6.8×10^{-2}	3.26×10^{-6}	0.0001
Al(2)–O_a	7×10^{-3}	3.9×10^{-6}	0.0031
Al(2)–O_c	1.85×10^{-2}	9.89×10^{-6}	0.0044
Al(2)–O_d	4×10^{-3}	2.2×10^{-6}	0.0082
Si–O_b	5×10^{-3}	3.0×10^{-6}	0.0043
Si–O_c	0	0	0.0154
Si–O_d	0	0	0.0124

Table 7. Calculated and observed valences and bond lengths for the wadsleyite (β-Mg_2SiO_4) structure

Bond	s_{calc}	$s_{calc.wt}$	R_{calc}, Å	$R_{calc.wt}$, Å	R_{obs}, Å
Mg(1)–O(3)	0.340	0.336	2.092	2.096	2.113
Mg(1)–O(4)	0.330	0.332	2.103	2.100	2.047
Mg(2)–O(1)	0.433	0.422	2.003	2.013	2.051
Mg(2)–O(2)	0.206	0.269	2.280	2.179	2.091
Mg(2)–O(4)	0.340	0.327	2.092	2.107	2.089
Mg(3)–O(1)	0.392	0.395	2.040	2.037	2.025
Mg(3)–O(3)	0.309	0.305	2.127	2.133	2.119
Mg(3)–O(4)	0.299	0.300	2.139	2.138	2.123
Si–O(2)	0.897	0.865	1.664	1.677	1.703
Si–O(3)	1.041	1.054	1.609	1.605	1.640
Si–O(4)	1.030	1.040	1.613	1.609	1.634

ine-type structure for orthosilicates containing bivalent cations (Mg_2SiO_4, Fe_2SiO_4, Ni_2SiO_4, etc.) are characterized by the ideal bond valence distributions corresponding to the values of the Pauling valence strengths: s(Mg–O) = 1/3, s(Si–O) = 1. The structure with such a simple distribution of bond valences should possess the highest possible symmetry, e.g., oxygen atoms in the structure should form the hexagonal close packing with half of the octahedral voids being filled with Mg atoms alternating in a chess-board order with vacancies, whereas Si atoms should be distributed over tetrahedra sharing no faces and edges with Mg-octahedra [70]. However, the real Mg_2SiO_4 structure consists of tetrahedra that do share their edges with the MgO_6-octahedra, thus giving rise to geometric strains and lowering the octahedron symmetry from the holohedral $m3m$ to $\bar{1}$ (in the position $M1$) and m (in the position $M2$) and the tetrahedron symmetry, from $\bar{4}3m$ to $mm2$.

Consider another example of the geometrically strained structure—the β-phase of wadsleyite β-Mg_2SiO_4 formed from forsterite α-Mg_2SiO_4 under pressures exceeding 13 GPa. The connectivity matrix for the structure can be written as

	O(1)	O(2)	O(3) (×2)	O(4) (×4)
Mg(1)	0	0	2	4
Mg(2)	1	1	0	4
Mg(3) (×2)	2	0	2	2
Si (×2)	0	1	1	2

It is seen that the O(2) atom is bound to two tetrahedrally coordinated Si atoms and one o Mg atom. This indicates that the O(2) atom is pronouncedly supersaturated with respect to Pauling valence strengths ($\sum s_i = 2.33$). This results in elongation of the Si–O(2) bond (1.703 Å) and formation of the very small Si–O(2)–Si bond angle (122°). On the other hand, the O(1) atom has five neighbors, 1Mg(2) + 4 Mg(3), forming a distorted square pyramid, and thus its valence is undersaturated with respect to the Pauling valence strength ($\sum s_i = 1.67$). To this position there corresponds a very low value of the electrostatic potential, 19.6 eV (compare with the average potential for O-atom equal to 28.6 eV) [71]. This signifies that in such a structure, there is, at least, one position appropriate for protonation and formation of a hydroxyl OH in the site O(1) (this was first assumed by Smyth in 1987 [72]).

The ideal valences and bond lengths obtained are listed in Table 7 together with the s and R values with due regard for the weighting scheme.

Comparing the calculated and the experimental bond lengths, we see that the most geometrically strained bonds in the structure are Mg(2)–O(2) and Si–O(2), whereas Mg(2)–O(1) and Mg(3)–O(1) are rather close to those predicted on the basis of our model. Indeed, the detailed analysis of the electrostatic potential obtained from the precision X-ray data [73] shows that the potential minimum is close to the position O(2), which indicates that this position, along with the position O(1), is most favorable for the protonation reaction. These assumptions are confirmed by the recent study of the Raman and the IR spectra of the β-phase $Mg_{1.74}Si_{0.97}H_{0.65}O_4$ [74].

Typical nonlocal geometric strains are observed in the perovskite-type structure described by the general formula ABO_3. The cuboctahedral coordination polyhedra of large A cations and octahedra of relatively small B cations share the edges, which results in the compression of the former and extension of the latter polyhedra. Thus, the octahedral voids become too large for B atoms, which, in accordance with the distortion theorem, are displaced from the centers of their polyhedra. As a result, such crystals show important ferroelectric properties. The equal-valence rule (27) is violated and, the bond valences deviate from their ideal values.

In some cases, geometric strains in the structure can be diminished or eliminated because of the occurrence

Table 8. Bond-strain factors in the $BaTiO_3$ structure

Structure symmetry	δ_{Ba-O}	δ_{Ti-O}	δ_{struct}
Orthorhombic	0.063	0.202	0.132
Trigonal	0.048	0.196	0.122
Tetragonal	0.061	0.064	0.063
Hexagonal	0.033	0.035	0.034
Cubic	0.060	0.060	0.060

of electronic effects. Thus, the combination of the "compressed" Bi–O layers and the CuO_2 layers in high-T_c superconductors is accompanied by the displacement of Bi atoms from the centers of their octahedra and formation of trigonally distorted coordination.

Sometimes, the bond-length relaxation initiates the electronic transitions between the cations possessing different valence states. Then, if such transitions result in the formation of advantageous electronic configurations, the energy spent on distortion of the structure reduces, and the positions are stabilized (e.g., the positions occupied by Cu^+, Cu^{2+}, and Cu^{3+} in the $BaY_2Cu_3O_7$ structure [75]).

Recently, it was shown [76] on an example of trivalent antimony in alkali metal and alkali earth thio- and selenoantimonates that the electronic effects for atoms with lone electron pairs can be taken into account within the framework of the bond valence method if one assumes that the parameter R_1 depends on the bond angle X–Sb–X, i.e., on the sp-hybridization of the valence orbitals of the Sb atom. The alternative method for interpreting the experimental data (almost equally accurate) consists in the withdrawal of the universal value $b = 0.37$ Å and the use of the individual values of this parameter for the Sb^{III}–S and Sb^{III}–Se bonds equal to 0.54 and 0.50 Å, respectively. An increase of the b values in this case can be attributed to the effect of repulsion of electrons of the lone-pair bonds and a higher "lability" of the corresponding bond lengths.

In some instances, the strains cannot be completely eliminated, and the valence-sum rule (4) is violated. The "residual strains" were revealed for some Al positions in β-alumina [77], in the melilite structure [78], and in La_2NiO_4 [79].

For the tetragonally distorted perovskite-type $BaTiO_3$ structure, the residual strains D [see (6)] attain the values of 0.35 v.u. This is explained by the too large size of a Ba atom (the parameter of the cubic unit cell corresponding to the unstrained Ba–O bond should be equal to $a = \sqrt{2}R(\text{Ba–O}) = 4.16$ Å), and a too small Ti atom (the parameter of the cubic unit cell corresponding to the unstrained Ti–O bond should be equal to $a = 2R(\text{Ti–O}) = 3.93$ Å). In the real structure, the Ba–O distances should be shortened, whereas the Ti–O distances, elongated. The unit-cell parameter is equal to the averaged value of the two above values. Under the compression of the structure as a whole at room temperature, the compromise is attained due to lowering of the structure symmetry. The residual strains seem to become even more pronounced with the lowering of the temperature T. The $BaTiO_3$ structure experiences even more pronounced distortion and, finally, at 5°C, it is transformed into the orthorhombic structure.

On the whole, the calculations [14] show that the structures stable at room temperature usually correspond to the condition $D < 0.2$ v.u. The structures with $D > 0.2$ v.u. are usually unstable and undergo phase transformation in order to reduce their D value. Thus, the residual-strain factor D seems to be a useful criterion for determining the crystal-structure stability.

As was indicated above, one can also use another indicator of the bond strain—the difference between the theoretically predicted and experimentally observed bond lengths. In this case, the strain factor δ for a certain group of bonds or the structure as a whole can be described by the formula

$$\delta = \sqrt{\frac{\sum_{i=1}^{N} (s_{i\,\text{theor}} - s_{i\,\text{exp}})^2}{N}},$$

where $s_{i\,\text{exp}}$ is the experimental value of the bond valence obtained from the experimental bond length by formula (3).

The δ values for various variants of the distortion of the perovskite-type $BaTiO_3$ structure are listed in Table 8 (δ_{Ba-O}, δ_{Ti-O}, and δ_{struct} are the strain factors for the groups of the Ba–O and Ti–O bonds and all the bonds in the structure, respectively).

4. CONCLUSION

The analysis of one of the crystallochemical procedures used for the interpretation and prediction of bond lengths in inorganic crystals, shows that, the modern bond-valence model can be successfully used at the initial stage of crystal-structure modeling. The simplicity of the mathematical apparatus used in the method and its numerous successful applications make it rather attractive and popular. However, the possibilities of the method are far from being fully used. The method is very promising and should be further developed.

To be able to predict interatomic distances in crystals, the program BONDVAL [80] based on the bond-valence method was written for IMB-compatible personal computers in Turbo Pascal 7.0 at the Crystallography and Crystal Chemistry Department of the Geology Faculty of the Moscow State University. All the BVM-based calculations analyzed in this study were performed using the BONDVAL program.

APPENDIX 1

Parameters of the bond-valence model for various atomic pairs

Atom	V_i	Atom	V_i	R_1, (2)	N, (2)	R_1, (3)	Atom	V_i	Atom	V_i	R_1, (2)	N, (2)	R_1, (3)
Ag	1	O	–2	1.946	7.4	1.842	Cu	2	F	–1	2.050	5.6	1.594
Ag	1	S	–2	2.080	5.8	2.119	Cu	2	O	–2	1.718	6.0	1.679
Al	3	Cl	–1			2.032	Cu	2	S	–2	2.095	7.2	2.054
Al	3	F	–1			1.545	D	1	O	–2			0.927
Al	3	O	–2			1.651	Dy	3	O	–2			2.001
As	3	O	–2			1.789	Er	3	F	–1			1.904
As	3	S	–2	2.280	4.3	2.272	Er	3	O	–2			1.988
As	5	F	–1			1.620	Eu	2	S	–2			2.584
As	5	O	–2			1.767	Eu	3	O	–2			2.074
B	3	F	–2			1.281	Fe	2	O	–2	1.764	5.5	1.734
B	3	O	–1			1.371	Fe	3	S	–2			1.689
Ba	2	F	–2	1.906	4.5	2.188	Fe	3	F	–1			1.679
Ba	2	O	–1	2.297	7.0	2.285	Fe	3	O	–2	1.780	5.7	1.759
Ba	2	S	–2			2.769	Fe	3	S	–2	2.138	5.4	2.149
Be	2	F	–1			1.281	Ga	3	O	–2			1.730
Be	2	O	–2			1.381	Ga	3	S	–2			2.163
Bi	3	O	–2	2.010	5.0	2.094	Ge	4	O	–2			1.748
Bi	3	S	–2	2.600	8.0	2.570	Ge	4	S	–2	2.210	2.4	2.217
C	4	N	–3			1.442	H	1	N	–3			0.885
C	4	O	–2	1.370	4.4	1.390	H	1	O	–2	0.870	2.2	0.882
Ca	2	F	–1	1.889	6.0	1.842	Hg	2	O	–2	1.983	6.5	1.972
Ca	2	O	–2	1.909	5.4	1.967	Hg	2	S	–2	2.223	5.0	2.308
Cd	2	Cl	–1	2.186	6.0	2.212	Ho	3	O	–2			2.025
Cd	2	O	–2	1.990	7.4	1.904	I	5	O	–2	1.967	4.5	2.003
Cd	2	S	–2	2.270	6.0	2.304	In	3	F	–1	1.835	6.3	1.792
Cl	7	O	–2	1.622	4.7	1.632	In	3	O	–2	1.959	7.0	1.902
Co	2	Cl	–1			2.033	In	3	S	–2	2.340	6.2	2.370
Co	2	O	–2	1.727	5.6	1.692	K	1	Cl	–1			2.519
Co	3	C	–2			1.634	K	1	F	–1	1.420	3.3	1.992
Cr	3	F	–1	1.700	6.5	1.657	K	1	O	–2	2.276	9.1	2.132
Cr	3	O	–2	1.733	5.2	1.724	La	3	O	–2	2.167	6.5	2.172
Cr	6	O	–2	1.787	5.0	1.794	La	3	S	–2			2.643
Cs	1	Cl	–1	3.020	12.8	2.791	Li	1	F	–1			1.360
Cs	1	O	–2	2.335	6.6	2.417	Li	1	O	–2			1.466
Cu	1	I	–1			2.108	Mg	2	F	–1			1.578
Cu	1	S	–2			1.898	Mg	2	O	–2			1.693

Table (Contd.)

Atom	V_i	Atom	V_i	R_1, (2)	N, (2)	R_1, (3)	Atom	V_i	Atom	V_i	R_1, (2)	N, (2)	R_1, (3)
Mn	2	Cl	–1			2.133	Sb	5	O	–2	1.911	6.0	1.942
Mn	2	F	–1	1.720	5.6	1.698	Sc	3	O	–2	1.865	5.4	1.849
Mn	2	O	–2	1.798	5.6	1.790	Sc	3	S	–2			2.321
Mn	3	O	–2	1.769	5.5	1.760	Se	4	O	–2	1.796	4.0	1.811
Mn	4	O	–2	1.774	5.2	1.753	Se	6	O	–2	1.775	5.0	1.788
Mo	6	O	–2	1.882	6.0	1.907	Si	4	C	–4			1.883
N	3	O	–2			1.361	Si	4	N	–3			1.724
N	5	O	–2	1.430	4.00	1.432	Si	4	O	–2			1.624
Na	1	F	–1			1.677	Si	4	S	–2			2.126
Na	1	O	–2			1.803	Sn	2	F	–1	1.739	3.5	1.925
Na	1	S	–2	1.532	4.29	2.300	Sn	4	Cl	–1			2.276
Nb	5	O	–2	1.907	5.0	1.911	Sn	4	F	–1	1.846	6.3	1.843
Nd	3	O	–2	2.137	6.5	2.105	Sn	4	O	–2	1.955	8.1	1.905
Ni	2	F	–1			1.596	Sn	4	S	–2	2.390	5.8	2.399
Ni	2	O	–2	1.680	5.4	1.654	Sr	2	O	–2	2.143	7.0	2.118
P	5	N	–3	1.700	4.8	1.704	Ta	5	O	–2	1.907	5.0	1.920
P	5	O	–2			1.617	Tb	3	O	–2	2.065	6.5	2.032
P	5	S	–2			2.145	Te	4	O	–2	1.933	4.5	1.977
Pb	2	O	–2	2.044	5.5	2.112	Te	6	O	–2	1.911	7.0	1.917
Pb	2	S	–2	2.265	7.9	2.541	Th	4	F	–1			2.068
Pb	4	O	–2			2.042	Ti	4	O	–2	1.806	5.2	1.815
Pr	3	O	–2	2.150	6.5	2.138	Tl	1	I	–1			2.822
Rt	2	C	–2			1.760	Tl	1	S	–2	2.220	5.0	2.545
Rt	4	O	–2			1.879	U	4	F	–1			2.038
Rb	1	Cl	–1	2.310	5.6	2.652	U	6	O	–2	2.059	4.3	2.075
Rb	1	O	–2	2.220	7.0	2.263	V	3	O	–2	1.762	5.2	1.743
S	2	N	–2	1.690	5.6	1.597	V	4	O	–2	1.770	5.2	1.784
S	2	N	–3			1.682	V	5	O	–2	1.791	5.1	1.803
S	4	N	–3			1.762	W	6	O	–2	1.904	6.0	1.917
S	4	O	–2	1.629	4.6	1.644	Y	3	O	–2	2.070	7.0	2.019
S	6	O	–2			1.624	Yb	3	O	–2			1.965
Sb	3	F	–1	1.772	3.7	1.883	Zn	2	Cl	–1			2.027
Sb	3	O	–2	1.910	4.5	1.973	Zn	2	O	–2			1.704
Sb	3	S	–2	2.450	6.0	2.474	Zr	4	F	–1			1.846
Sb	5	F	–1	1.830	7.3	1.797	Zr	4	O	–2	1.950	6.0	1.928

Note: The R_1 and N parameters for equation (2) are taken from [8–10], the parameters R_1 for equation (3) are taken from [15, 18]; b = 0.37 Å for all the pairs of atoms.

APPENDIX 2

Theoretically predicted bond lengths for some structures

Bond	Bond valence	Bond length, Å		Bond	Bond valence	Bond length, Å	
		calc.	obs.			calc.	obs.
	$Sr_3Ti_2O_7$				$KFeFPO_4$		
Sr(1)–O(1)	0.1704	2.772	2.760	K(1)–O(1)	0.116	2.929	3.060
Sr(1)–O(3)	0.1647	2.785	2.764	K(1)–O(2)	0.124	2.904	3.010
Sr(2)–O(2)	0.2546	2.624	2.651	K(1)–O(3)	0.124	2.904	2.917
Sr(2)–O(3)	0.1816	2.749	2.766	K(1)–O(5)	0.162	2.805	3.085
Ti–O(1)	0.6591	1.969	1.964	K(1)–O(6)	0.121	2.913	3.032
Ti–O(2)	0.7265	1.933	1.951	K(1)–O(7)	0.129	2.889	2.832
Ti–O(3)	0.6535	1.972	1.976	K(1)–O(8)	0.121	2.913	2.723
	$Ba_2FeSi_2O_7$ (hardystonite)			K(1)–F(1)	0.052	3.084	2.677
Ba–O(1)	0.113	3.090	2.820	K(1)–F(2)	0.052	3.084	3.044
Ba–O(2)	0.306	2.723	2.730	K(2)–O(1)	0.136	2.870	2.707
Ba–O(3)	0.242	2.810	2.820	K(2)–O(2)	0.144	2.849	2.751
Fe–O(3)	0.500	1.990	1.960	K(2)–O(3)	0.144	2.849	3.079
Si–O(1)	0.887	1.668	1.630	K(2)–O(6)	0.141	2.856	2.709
Si–O(2)	1.081	1.595	1.560	K(2)–O(7)	0.149	2.836	2.870
Si–O(3)	1.016	1.618	1.630	K(2)–O(8)	0.141	2.856	2.887
	$Sr_3Zr_2O_7$			K(2)–F(1)	0.072	2.965	2.924
Sr(1)–O(1)	0.1704	2.772	2.754	K(2)–F(2)	0.072	2.965	2.632
Sr(1)–O(3)	0.1647	2.785	2.804	P(1)–O(2)	1.213	1.546	1.543
Sr(2)–O(2)	0.2546	2.624	2.716	P(1)–O(3)	1.213	1.546	1.548
Sr(2)–O(3)	0.1816	2.749		P(1)–O(4)	1.356	1.504	1.532
Zr–O(1)	0.6591	2.082	2.053	P(1)–O(7)	1.218	1.544	1.538
Zr–O(2)	0.7265	2.046	2.017	P(2)–O(1)	1.236	1.538	1.535
Zr–O(3)	0.6535	2.085	2.063	P(2)–O(5)	1.282	1.525	1.531
	$Y_2SiBe_2O_7$			P(2)–O(6)	1.241	1.537	1.545
Y–O(1)	0.439	2.327	2.340	P(2)–O(8)	1.241	1.537	1.545
Y–O(2)	0.467	2.300	2.306	Fe(1)–O(4)	0.641	1.923	1.956
Y–O(3)	0.290	2.477	2.450	Fe(1)–O(6)	0.947	1.779	1.923
Si–O(3)	1.128	1.624	1.670	Fe(1)–O(7)	0.505	2.011	2.032
Be–O(1)	0.563	1.593	1.560	Fe(1)–O(8)	0.947	1.779	1.947
Be–O(2)	0.596	1.572	1.550	Fe(1)–F(1)	0.428	1.992	2.034
Be–O(3)	0.418	1.703	1.710	Fe(1)–F(2)	0.428	1.992	2.009
				Fe(2)–O(1)	0.511	1.982	2.049
				Fe(2)–O(2)	0.519	1.976	1.975
				Fe(2)–O(3)	0.519	1.976	1.962
				Fe(2)–O(5)	0.557	1.950	1.993
				Fe(2)–F(1)	0.447	1.976	1.968
				Fe(2)–F(2)	0.447	1.976	1.993

ACKNOWLEDGMENTS

The authors are grateful to K.A. Popov for his help in writing the program. The study was supported by State Program for the Leading Scientific Schools, project no. 96-15-98315.

REFERENCES

1. Urusov, V.S., *Teoreticheskaya kristallokhimiya* (Theoretical Crystal Chemistry), Moscow: Mosk. Gos. Univ., 1987.
2. Zachariasen, W.H., *Acta Crystallogr.*, 1954, vol. 7, p. 795.
3. Smith, J.V., *Am. Mineral.*, 1953, vol. 38, p. 643.
4. Donnay, G. and Allmann, R., *Am. Mineral.*, 1970, vol. 55, p. 1003.
5. Baur, W.H., *Trans. Amer. Crystallogr. Assoc*, 1970, vol. 6, p. 129.
6. Nyburg, S., *J. Cryst. Molec. Struct*, 1973, vol. 3, p. 331.
7. Pyatenko, Yu.A., *Kristallografiya*, 1972, vol. 17, p. 773.
8. Brown, I.D. and Shannon, R.D., *Acta Crystallogr., Sect. A: Cryst. Phys., Diffr., Theor. Gen. Crystallogr.*, 1973, vol. 29, p. 266.
9. Brown, I.D. and Wu, K.K., *Acta Crystallogr. Sect. B: Struct. Crystallogr. Crystal Chem*, 1976, vol. 32. p. 1957.
10. Brown, I.D., *Structure and Bonding in Crystals*, O'Keeffe, M. and Navrotsky, A. Eds., New York: Academic, 1981.
11. Allmann, R., *Monatsh. Chem.*, 1975, vol. 106, p. 779.
12. Zachariasen, W.H., *J. Less-Common Met.*, 1978, vol. 62, p. 1.
13. Pauling, L., *J. Am. Chem. Soc.*, 1947, vol. 69, p. 541.
14. Brown, I.D., *Acta Crystallogr., Sect. B: Struct. Sci.*, 1992, vol. 48, p. 553.
15. Brown, I.D. and Altermatt, D., *Acta Crystallogr., Sect. B: Struct. Sci.*, 1985, vol. 41, p. 244.
16. Bergerhoff, G., Hundt, R., Sievers, R., and Brown, I.D., *J. Chem. Comput. Sci*, 1983, vol. 23, p. 66.
17. Breese, N.E. and O'Keeffe, M., *Acta Crystallogr., Sect. B: Struct. Sci.*, 1991, vol. 47, p. 192.
18. O'Keeffe, M. and Breese, N.E., *J. Am. Chem. Soc.*, 1991, vol. 110, p. 1506.
19. Brown, I.D., *Chem. Soc. Rev.*, 1978, vol. 7, p. 354.
20. Brown, I.D., *Acta Crystallogr., Sect. B: Struct. Sci.*, 1992, vol. 8, p. 553.
21. Kudoh, Y., Ito, E., and Takeda, H., *Phys. Chem. Minerals*, 1987, vol. 14, p. 350.
22. Urusov, V.S. and Orlov, I.P., *Spektroskopiya, rentgenografiya i kristallokhimiya mineralov* (Spectroscopy, X-ray Diffraction, and Crystal Chemistry of Minerals), Kazan: Kazan. Univ., 1997, p. 3.
23. Bürgi, H.B., *Angew. Chem.*, 1975, vol. 87, p. 461.
24. Gazo, J., Bersuker, I., Garaj, J., *et al.*, *Coord. Chem. Rev.*, 1976, vol. 19, p. 253.
25. Gazo, J., Boca, R., Jona, E., *et al.*, *Coord. Chem. Rev.*, 1982, vol. 43, p. 87.
26. Gazo, J., Boca, R., Jona, E., *et al.*, *Pure Appl. Chem.*, 1983, vol. 55, p. 65.
27. Hathaway, B.J., *Struct. Bonding*, 1973, vol. 14, p. 49.
28. Murray-Rust, P., Bürgi, H.B., and Dunitz, J.D., *Acta Crystallogr., Sect. B: Struct. Crystallogr. Cryst. Chem.*, 1978, vol. 34, p. 1787.
29. Boca, R., *Polyhedron*, 1995, vol. 14, no. 3, p. 367.
30. Jansen, L., Chandran, L., and Block, R., *J. Mol. Struct.*, 1992, vol. 250, p. 81.
31. Urusov, V.S., *Acta Crystallogr., Sect. B: Struct. Sci.*, 1995, vol. 51, p. 641.
32. Urusov, V.S., *Dokl. Akad. Nauk.*, 1996, vol. 349, no. 5, p. 644.
33. Bürgi, H.-B. and Dunitz, J., *J. Am. Chem. Soc.*, 1987, vol. 109, p. 2924.
34. Brown, I.D., *Acta Crystallogr., Sect. B: Struct. Crystallogr. Cryst. Chem.*, 1977, vol. 33, p. 1305.
35. Phillips, M.W., Gibbs, G.V., and Ribbe, P.H., *Am. Mineral.*, 1974, vol. 59, p. 79.
36. Urusov, V.S. and Orlov, I.P., *Dokl. Akad. Nauk.*, 1997, vol. 353, no. 1, p. 66.
37. Rutherford, J.S., *Acta Crystallogr., Sect. B: Struct. Sci.*, 1990, vol. 46, p. 289.
38. Urusov, V.S., Dubrovinskaya, N.A., and Dubrovinskii, L.S., *Konstruirovanie veroyatnykh kristallicheskikh struktur mineralov* (Construction of Probable Crystal Structures of Minerals), Moscow: Mosk. Gos. Univ., 1990.
39. Walterson, K., *Acta Crystallogr., Sect. A: Cryst. Phys., Diffr., Theor. Gen. Crystallogr.*, 1978, vol. 34, p. 901.
40. Brown, I.D., *Solid State Ionics*, 1988, vol. 31, p. 203.
41. Dubrovinskii, L.S., Korovina, I.A., and Urusov, V.S., *Mineralogicheskii sbornik.* L'viv, 1991, vol. 1, no. 45, p. 3.
42. Yamanaka, Y., Toronami, M., and Taruichi, Y., *Acta Crystallogr., Sect. B: Struct. Sci.*, 1984, vol. 40, p. 96.
43. *Hard and Soft Acids and Bases*, Pearson, R.G., Ed., Strasbourg, PA: Dowden, Hutchinson & Ross, 1973.
44. Urusov, V.S., *Energeticheskaya kristallokhimiya* (Energetic Crystal Chemistry), Moscow: Nauka, 1975.
45. Brown, I.D., *Acta Crystallogr., Sect. B: Struct. Sci.*, 1988, vol. 44, p. 545.
46. Brown, I.D. and Skowron, A., *J. Am. Chem. Soc.*, 1990, vol. 112, p. 3401.
47. Dent-Glasser, L., *Z. Kristallogr.*, 1979, vol. 149, p. 291.
48. Pyatenko, Yu.A., *Izv. Akad. Nauk SSSR, Ser. Geol.*, 1983, no. 8, p. 3.
49. Pyatenko, Yu.A., *Kristallografiya i kristallokhimiya* (Crystallography and Crystal Chemistry), Moscow: Nauka, 1986, p. 158.
50. Hawthorne, F., *Can. Mineral.*, 1997, vol. 35, p. 201.
51. Kharisin, M.R., Taylor, D.J., Bevan, M., and Pring, A., *Mineral. Mag*, 1996, vol. 60, no. 5, p. 833.
52. O'Keeffe, M., *Structure and Bonding in Crystals*, 1989, vol. 1, p. 299.
53. Brown, I.D., *J. Solid State Chem.*, 1991, vol. 90, p. 155.
54. Thorp, H.H., *Inorg. Chem.*, 1992, vol. 31, p. 1585.
55. Liu, W. and Thorp, H.H., *Inorg. Chem.*, 1993, vol. 32, p. 4102.
56. Scarrow, R.L., Tiimitsis, M.G., Buck, C.P., *et al.*, *Biochem*, 1994, vol. 33, p. 15023.

57. Shu, L., Chion, Y.-M., Orville, A.M., *et al.*, *Biochem*, 1995, vol. 34, p. 6649.
58. Sironi, A., *Inorg. Chem.*, 1995, vol. 34, p. 1342.
59. Duan, C.-Y., Tian, Y.-P., Lu, Z.-L., and You, X.-Z., *Inorg. Chem.*, 1995, vol. 34, p. 1412.
60. Khudolozhkin, V.O., Urusov, V.S., and Tobelko, K.I., *Geokhimiya*, 1973, no. 11, p. 1610.
61. Urusov, V.S. and Khudolozhkin, V.O., *Geokhimiya*, 1974, no. 10, p. 1509.
62. Hughes, J.M., Cameron, M., and Mariano, A.N., *Am. Mineral.*, 1991, vol. 76, p. 1165.
63. Fleet, M.E. and Pan, Y., *Am. Mineral.*, 1995, vol. 80, p. 329.
64. Urusov, V.S., *Teoriya izomorfnoi smesimosti* (Theory of Isomorphic Mixing), Moscow: Nauka, 1977.
65. Fleet, M.E. and Pan, Y., *Eur. J. Mineral.*, 1995, vol. 7, p. 591.
66. Ziolkowski, J., *J. Catal.*, 1983, vol. 84, p. 317.
67. Ziolkowski, J. and Dziembaj, L., *J. Solid State Chem.*, 1985, vol. 57, p. 291.
68. Winter, J.K. and Chose, S., *Am. Mineral.*, 1979, vol. 64, p. 573.
69. Brown, I.D., Dabkowski, A., and McCleary, A., *Acta Crystallogr., Sect. B: Struct. Sci.*, 1997, vol. 53, p. 750.
70. Bragg, W.L. and Claringbull, G.S., *Crystal Structure of Minerals*, London: G.Bell and Sons, 1965. Translated under the title *Kristallicheskaya struktura mineralov*, Moscow: Mir, 1967.
71. Smyth, J.R., *Geochim. Cosmochim. Acta*, vol. 53, p. 1101.
72. Smyth, J.R., *Am. Mineral.*, 1987, vol. 72, p. 1051.
73. Downs, J.W., *Am. Mineral.*, 1989, vol. 74, p. 1124.
74. Mernagh, T.P. and Liu, L.-G., *Can. Mineral.*, 1996, vol. 34, p. 1233.
75. Brown, I.D., *J. Solid State Chem*, 1991, vol. 90, p. 155.
76. O'Keeffe, M. and Brese, N.E., *Acta Crystallogr., Sect. B: Struct. Sci.*, 1992, vol. 48, p. 152.
77. Wagner, T.R. and O'Keeffe, M., *J. Solid State Chem.*, 1988, vol. 73, p. 211.
78. Armbruster, T., Rothlisberger, F., and Seifert, F., *Am. Mineral.*, 1990, vol. 75, p. 847.
79. Brown, I.D., *Z. Kristallogr.*, 1991, vol. 199, p. 255.
80. Orlov, I.P., Popov, K.A., and Urusov, V.S., *Zh. Strukt. Khim.*, 1998, vol. 39, no. 4, p. 706.

Translated by L. Man